METEOROLOGICAL OFFICE
4 JUL 1990
LIBRARY

METEOROLOGICAL OFFICE COLLEGE

FRONTS

D. A. BENNETTS
M. J. P. CULLEN

ORGS UKMO A

National Meteorological Library
FitzRoy Road, Exeter, Devon. EX1 3PB

Headquarters, Bracknell

FRONTS

1. Introduction

Frontal systems are probably the best known of all meteorological phenomena. They occur at the boundaries of air masses and are generally characterised by bands of cloud and rain. Their overall structure is well described by the 'Norwegian' models and although these were developed more than 50 years ago they are still useful today. However, during the past 15-20 years there has been considerable interest in the wide variety of meso-scale phenomena that develop within or near frontal zones. Much of the knowledge of these features has been gained through radar observations (both conventional and doppler), dropsondes, special radiosondes and research aircraft.

The aim of these notes is to outline some of the results of this recent research and to place it in context with more established frontal theory. They are divided into six sections

a. Classical theory of frontal systems
b. Frontogenesis
c. Geometrical interpretation of fronts and frontogenesis
d. The structure of extra-tropical cyclones
e. Theory of meso-scale instabilities
f. Observation of mesoscale instabilities.

2. Classical theory of frontal systems

In frontal zones there are large variations over small distances. Hence, to a first order of approximation, we may think of a front as a discontinuity.

To find the equilibrium slope of a frontal surface, consider adjacent air masses with the surface front lying parallel to the y axis (Figure 1).

Let the variables in the cold air have suffices 1 and those in the warm air suffices 2.

Consider the small rectangle abcd.

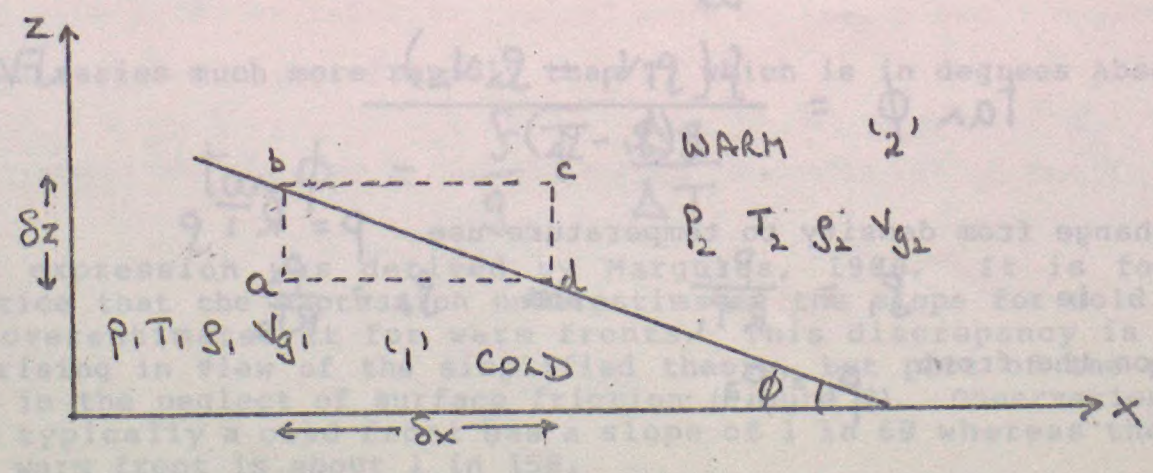

Figure 1. Margules concept of an atmospheric front.

$$\left(\frac{dp}{dx}\right)_1 = \frac{p_a - p_d}{\delta x} \; ; \; \left(\frac{dp}{dx}\right)_2 = \frac{p_b - p_c}{\delta x}$$

Now $p_a = p_b + \rho_1 g \delta z$

$p_c = p_d - \rho_2 g \delta z$

So $\left(\frac{dp}{dx}\right)_2 - \left(\frac{dp}{dx}\right)_1 = \frac{p_b - p_a - (p_c - p_d)}{\delta x}$

$$= \frac{-\rho_1 g \delta z + \rho_2 g \delta z}{\delta x}$$

$$= -g(\rho_1 - \rho_2)\frac{\delta z}{\delta x} .$$

Re-arranging

$$\frac{\delta z}{\delta x} = \tan\phi = \frac{\left(\frac{dp}{dx}\right)_1 - \left(\frac{dp}{dx}\right)_2}{g(\rho_1 - \rho_2)} \qquad (F.1)$$

If we assume the flow is geostrophic

$$V_1 = \frac{1}{\rho_1 f}\left(\frac{dp}{dx}\right)_1 \quad \text{and} \quad V_2 = \frac{1}{\rho_2 f}\left(\frac{dp}{dx}\right)_2$$

where V flows parallel to the surface fronts.

Substitute in (F.1) for $\frac{dp}{dx}$

$$\tan\phi = \frac{f(\rho_1 V_1 - \rho_2 V_2)}{g(\rho_1 - \rho_2)} \qquad (F.2)$$

To change from density to temperature use $p = RT\rho$

ie $\rho_1 = \frac{p_1}{RT_1}$ and $\rho_2 = \frac{p_2}{RT_2}$

and on the front $p_1 = p_2$.

So $\rho_1 \propto \frac{1}{T_1}$ and (F.2) becomes

$$\tan\phi = \frac{f}{g}\left\{\frac{\frac{V_1}{T_1}}{\frac{1}{T_1}-\frac{1}{T_2}} - \frac{\frac{V_2}{T_2}}{\frac{1}{T_1}-\frac{1}{T_2}}\right\}$$

$$= \frac{f}{g}\left\{\frac{V_1}{T_1\left(\frac{T_2-T_1}{T_1T_2}\right)} - \frac{V_2}{T_2\left(\frac{T_2-T_1}{T_1T_2}\right)}\right\}$$

$$\tan\phi = \frac{f}{g}\left\{\frac{T_2V_1}{T_2-T_1} - \frac{T_1V_2}{T_2-T_1}\right\} \quad (F.3)$$

But V varies much more rapidly than T, which is in degrees Absolute

so $$\tan\phi = \frac{f}{g}\,\overline{T}\,\frac{\Delta V}{\Delta T}. \quad (F.4)$$

This expression was derived by Margules, 1906. It is found in practice that the expression underestimates the slope for cold fronts and overestimates it for warm fronts. This discrepancy is hardly surprising in view of the simplified theory, but part of the problem lies in the neglect of surface friction (Figure 2). Observations show that typically a cold front has a slope of 1 in 60 whereas the slope of a warm front is about 1 in 150.

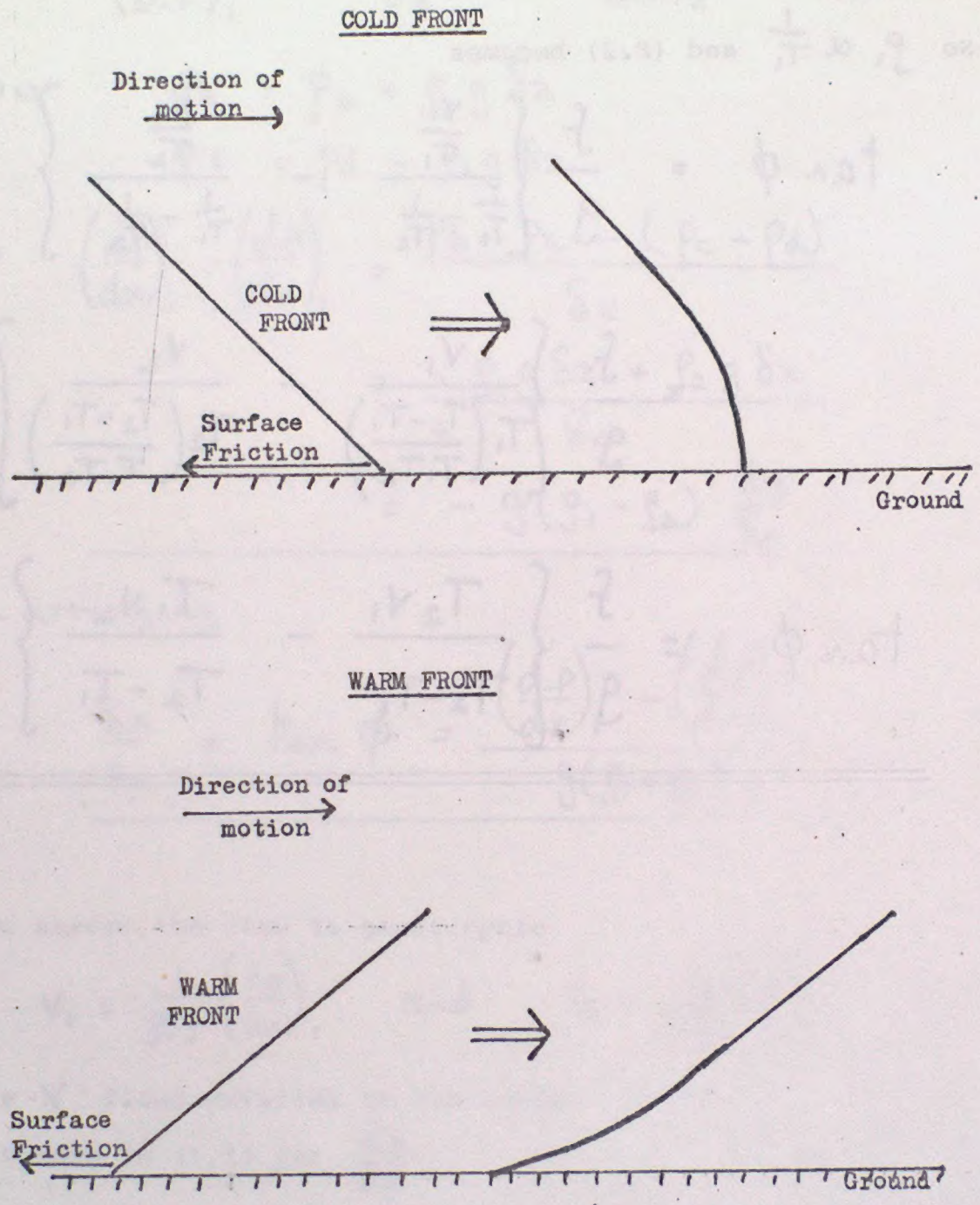

Figure 2. The effects of surface friction on warm and cold fronts.

The Margules solution is for geostrophic flow. But it is well known that within frontal zones the ageostrophic component of flow is also important. To examine this aspect of the flow we consider the full equations of motion which may be written.

$$\left.\begin{aligned} \frac{du}{dt} - fv + \frac{1}{\rho}\frac{\partial p}{\partial x} &= 0 \\ \frac{dv}{dt} + fu + \frac{1}{\rho}\frac{\partial p}{\partial y} &= 0 \end{aligned}\right\} \text{horizontal momentum} \qquad (F.5)$$

$$\frac{d\theta}{dt} = 0 \qquad \text{Conservation of Potential temperature} \qquad (F.6)$$

$$\frac{\partial v}{\partial z'} = \frac{g}{f\theta_0}\frac{\partial \theta}{\partial x}, \quad \frac{\partial u}{\partial z'} = \frac{g}{f\theta_0}\frac{\partial \theta}{\partial y} \qquad \text{Thermal wind} \qquad (F.7)$$

$$\frac{\partial u}{\partial x} + \frac{\partial v}{\partial y} + \frac{\partial w}{\partial z'} = 0 \qquad \text{Continuity} \qquad (F.8)$$

$$\frac{d}{dt} = \frac{\partial}{\partial t} + u\frac{\partial}{\partial x} + v\frac{\partial}{\partial y} + w\frac{\partial}{\partial z'} \qquad (F.9)$$

The use of pressure as a vertical ordinate provides a considerable simplification to the equations of motion. However it is not always the best quantity for intuitive understanding. A quantity that combines many of the advantages of both pressure and height is

$$z' = \left\{1 - \left(\frac{p}{p_0}\right)^k\right\}\frac{H_s}{k}$$

The scale height $H_s = p_0/\rho_0 g = R\theta_0/g$

where zero suffices refer to typical 1000 mb values and K = R/Cp.

Consider the quantity $\theta\, dz'$

$$\theta\, dz' = -\theta\left(\frac{p}{p_0}\right)^{k-1}\frac{1}{p_0}\frac{H_s}{k}k\, dp \qquad \left(\theta = \left(\frac{p_0}{p}\right)^k T\right)$$

$$= -T\left(\frac{p}{p_0}\right)^{k-1}\left(\frac{p_0}{p}\right)^k\frac{H_s}{p_0}\, dp$$

$$= -\frac{T H_s}{p}\, dp$$

$$\underline{\theta\, dz' = \theta_0\, d(\text{height})}$$

Therefore z' is almost identical to physical height.

$\Theta_o = 283^\circ$, R = 287, g = 9.81 Hs = 8279, k = 0.2856

height (m)	P (mb)	Z'
1000	898	980
2000	795	1938
3000	701	2893
4000	615	3851
6000	464	5794
8000	357	7467

This slight difference between Z' and physical height shows itself in the equation for the geopotential heights(ϕ)

Recall $$\frac{\partial \phi}{\partial(\text{height})} = g$$

$$\frac{\partial \phi}{\partial z'} \frac{\partial z'}{\partial(\text{height})} = g$$

or $$\frac{\partial \phi}{\partial z'} = \frac{g\Theta}{\Theta_o}$$

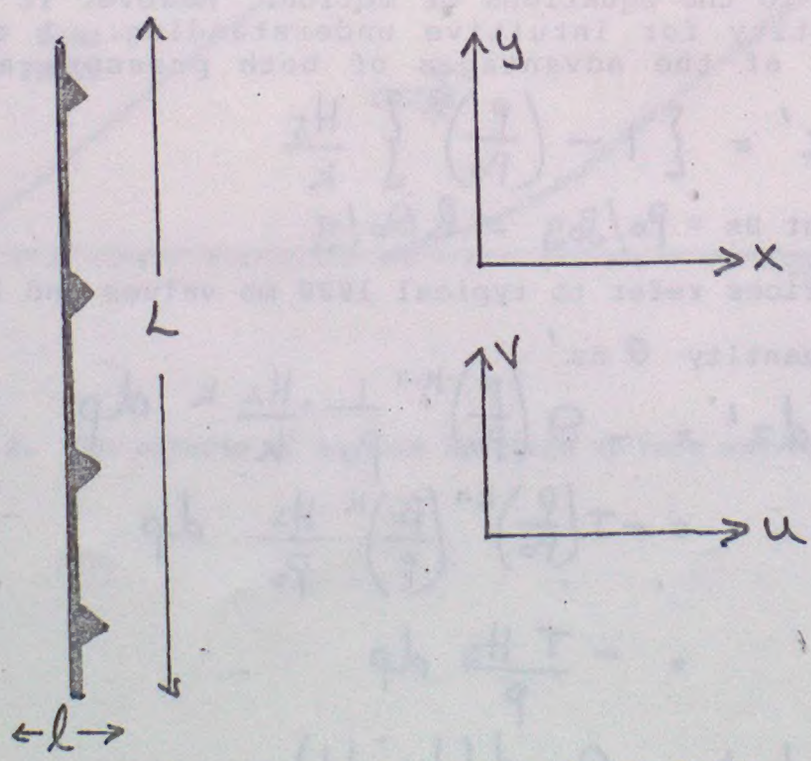

Figure 3. Scales relative to an atmospheric front.

Observations of atmospheric fronts show that (figure 3) relative to the front $V \gg u$ (we are now considering motion RELATIVE to the front) and of course $L \gg l$. Assuming that $d/dt \sim u/L$, then the ratio of the acceleration to the Coriolis force, in the x-direction, is

$$\frac{du/dt}{fv} \sim \frac{u^2/L}{fV} = \left(\frac{u}{V}\right)^2 \frac{V}{fL} \ll 1 \quad \left\{\begin{matrix} V \sim 20\,ms^{-1} \\ L \sim 200\,km \end{matrix}\right\}$$

and, in the y-direction, is

$$\frac{dv/dt}{fu} \sim \frac{uv/L}{fu} = \frac{V}{fL} \sim 1.$$

Thus we may use geostrophic balance (ie no acceleration) in the cross-frontal direction but not along the front. By also neglecting derivatives in the y direction, except $\partial p/\partial y$, ie considering a two dimensional front with no change in the y direction, the equations reduce the form,

$$\frac{dv}{dt} + fu + \frac{1}{\rho}\frac{\partial p}{\partial y} = 0 \qquad (F.10)$$

$$\frac{d\theta}{dt} = 0 \qquad (F.11)$$

$$\frac{\partial v}{\partial z} = \frac{g}{f\theta_0}\frac{\partial \theta}{\partial x}, \quad \frac{\partial u}{\partial z} = \frac{g}{f\theta_0}\frac{\partial \theta}{\partial y} \qquad (F.12)$$

$$\frac{\partial u}{\partial x} + \frac{\partial w}{\partial z} = 0 \qquad (F.13)$$

$$\frac{d}{dt} = \frac{\partial}{\partial t} + u\frac{\partial}{\partial x} + w\frac{\partial}{\partial z} \qquad (F.14)$$

Write $U = U_g + u'$, $V = V_g + V'$. Where the suffix 'g' refers to the geostrophic component of the flow and primes the ageostrophic component.

But, since the flow is geostrophic in the cross-frontal directions, $V' \equiv 0$.

Substitute into the horizontal momentum equation (F.10) and expand.

$$\frac{\partial V_g}{\partial t} + (U_g + u')\frac{\partial V_g}{\partial x} + V_g\frac{\partial V_g}{\partial y} + w\frac{\partial V_g}{\partial z} + fU_g + fu' + \frac{1}{\rho}\frac{\partial p}{\partial y} = 0 \qquad (F.18)$$

(for completeness)

To 1st order there is geostrophic balance

$$fU_g + \frac{1}{\rho}\frac{\partial p}{\partial y} = 0 \qquad (U_g = \text{speed of front})$$

and to 2nd order

$$\frac{\partial V_g}{\partial t} + U_g\frac{\partial V_g}{\partial x} + V_g\frac{\partial V_g}{\partial y} + u'\frac{\partial V_g}{\partial x} + w\frac{\partial V_g}{\partial z} + fu' = 0 \qquad (F.17)$$

Take $\frac{\partial}{\partial z}$ (F.17) and multiply by f

$$\frac{d}{dt}\left(f\frac{\partial V_g}{\partial z}\right) + f\frac{\partial U_g}{\partial z}\frac{\partial V_g}{\partial x} + f\frac{\partial V_g}{\partial z}\frac{\partial V_g}{\partial y} + f\frac{\partial u'}{\partial z}\frac{\partial V_g}{\partial x} + f\frac{\partial w}{\partial z}\frac{\partial V_g}{\partial z} + f^2\frac{\partial u'}{\partial z} = 0$$

$$\text{or } \frac{d}{dt}\left(f\frac{\partial V_g}{\partial z}\right) = -f\left(f + \frac{\partial V_g}{\partial x}\right)\frac{\partial u'}{\partial z} - f\frac{\partial V_g}{\partial z}\frac{\partial w}{\partial z} - f\frac{\partial U_g}{\partial z}\frac{\partial V_g}{\partial x} - f\frac{\partial V_g}{\partial z}\frac{\partial V_g}{\partial y} \qquad (F.$$

In a similar manner the thermodynamic equation can be expanded and differentiated with respect to x giving

$$\frac{d}{dt}\left(\frac{g}{\theta_0}\frac{\partial \theta}{\partial x}\right) = -\frac{g}{\theta_0}\frac{\partial \theta}{\partial x}\frac{\partial u'}{\partial x} - \frac{g}{\theta_0}\frac{\partial \theta}{\partial z}\frac{\partial w}{\partial x} - \frac{\partial U_g}{\partial x}\frac{g}{\theta_0}\frac{\partial \theta}{\partial x} - \frac{\partial V_g}{\partial x}\frac{g}{\theta_0}\frac{\partial \theta}{\partial y} \qquad (F.19)$$

Locally, the geostrophic variable can be considered constant and we may write

$$N^2 = \frac{g}{\theta_0}\frac{\partial \theta}{\partial z}, \quad S^2 = \frac{g}{\theta_0}\frac{\partial \theta}{\partial x} = f\frac{\partial V_g}{\partial z}, \quad F^2 = f\left(f + \frac{\partial V_g}{\partial x}\right)$$

and $$Q = -\frac{\partial U_g}{\partial x}\frac{g}{\theta_0}\frac{\partial \theta}{\partial x} - \frac{\partial V_g}{\partial x}\frac{g}{\theta_0}\frac{\partial \theta}{\partial y}$$

So that (F.18) and (F.19) become

$$\frac{d}{dt}\left(f\frac{\partial v_g}{\partial z}\right) = -Q - F^2\frac{\partial u'}{\partial z} - S^2\frac{\partial w}{\partial z} \qquad (F.20)$$

$$\frac{d}{dt}\left(\frac{g}{\theta_0}\frac{\partial \theta}{\partial x}\right) = Q - S^2\frac{\partial u'}{\partial x} - N^2\frac{\partial w}{\partial x} \qquad (F.21)$$

But in a frontal zone, thermal wind balance is <u>always</u> maintained and therefore, by writing

$$u' = \frac{\partial \psi}{\partial z}, \quad w = -\frac{\partial \psi}{\partial x} \qquad (v'=0)$$

(F.20) and (F.21) become

$$F^2\frac{\partial^2\psi}{\partial z^2} - 2S^2\frac{\partial^2\psi}{\partial x\partial z} + N^2\frac{\partial^2\psi}{\partial x^2} = -2Q \qquad (F.22)$$

Provided $S^4 < F^2N^2$ the equation is elliptic, and hence the streamlines form ellipses, the direction and strength of the circulation being determined by the sign and magnitude of Q.

Recall that for elliptic motion.

$$\frac{S^4}{F^2N^2} = f^2\left(\frac{\partial v_g}{\partial z}\right)^2 \Big/ f\left(f+\frac{\partial v}{\partial x}\right)\frac{g}{\theta_0}\frac{\partial \theta}{\partial z} = \frac{f\frac{\partial v_g}{\partial z}\frac{g}{\theta_0}\frac{\partial \theta}{\partial x}}{f\left(f+\frac{\partial v}{\partial x}\right)\frac{g}{\theta_0}\frac{\partial \theta}{\partial z}}$$

$$= \frac{\frac{\partial \theta}{\partial x}}{\frac{\partial \theta}{\partial z}} \cdot \frac{\frac{\partial v_g}{\partial z}}{f+\frac{\partial v_g}{\partial x}}$$

Let $X = x + v_g/f$ $\therefore \frac{\partial v_g}{\partial z} = f\frac{\partial X}{\partial z}$ and $f+\frac{\partial v_g}{\partial x} = f\frac{\partial X}{\partial x}$.

$$\therefore \frac{S^2}{F^2N^2} = \left(\frac{\delta z}{\delta x}\right)_\theta \Big/ \left(\frac{\delta z}{\delta x}\right)_X \qquad (F.23)$$

Clearly X is an important quantity.

Following Eliassen (1962) and Hoskins (1978)

Let $$X = x + V_g/f$$

the equation may be rewritten

$$f^2 \frac{\partial^2 \psi}{\partial z^2} + \frac{\partial}{\partial x}\left(q \frac{\partial \psi}{\partial x}\right) = -\frac{2Q}{\left(1 + f^{-1}\frac{\partial v_g}{\partial x}\right)} \qquad (F.24)$$

where q = Ertels potential vorticity ($dq/dt = 0$ following a fluid particle). For a closed streamline around a region where Q>0, the circulation within a cold front is shown below, in Figure 4a.

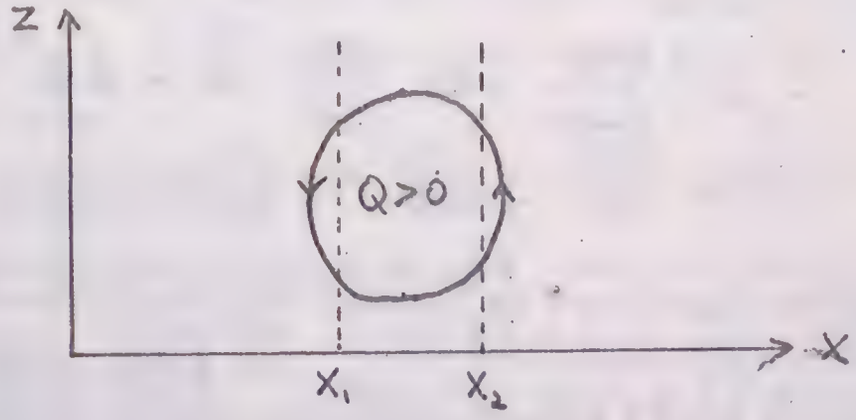

Fig 4a

To transform back to (X,Z) coordinates consider a cold frontal zone.

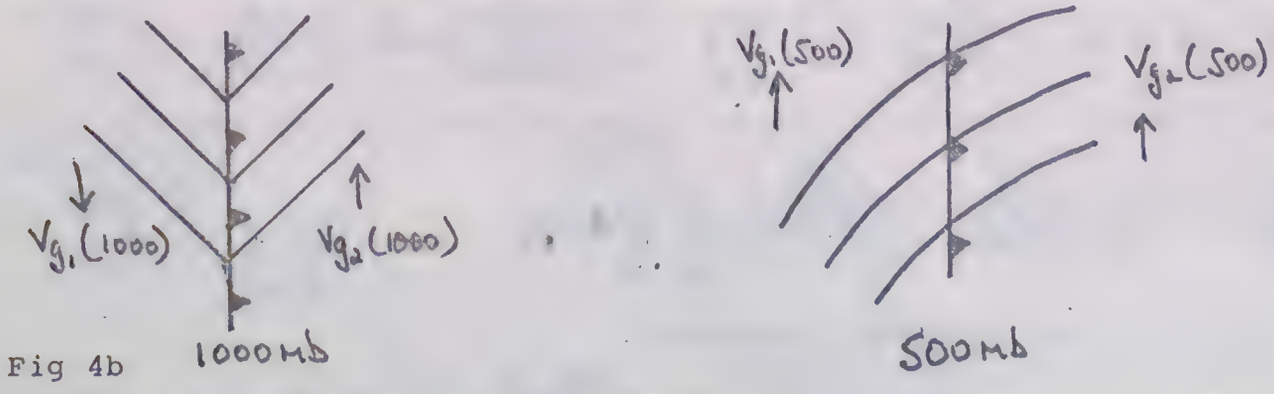

Fig 4b

at 1000 mb $x_1 = X_1 + Vg_1(1000)/f$ $x_2 = X_2 - Vg_2(1000)/f$

at 500 mb $x_1 = X_1 - Vg_1(500)/f$ $x_2 = X_2 - Vg_2(500)/f$

ie at the surface

X_1 moves right

X_2 moves left

at 500 mb

X_1 moves left

X_2 moves left

and the resulting streamline is shown below

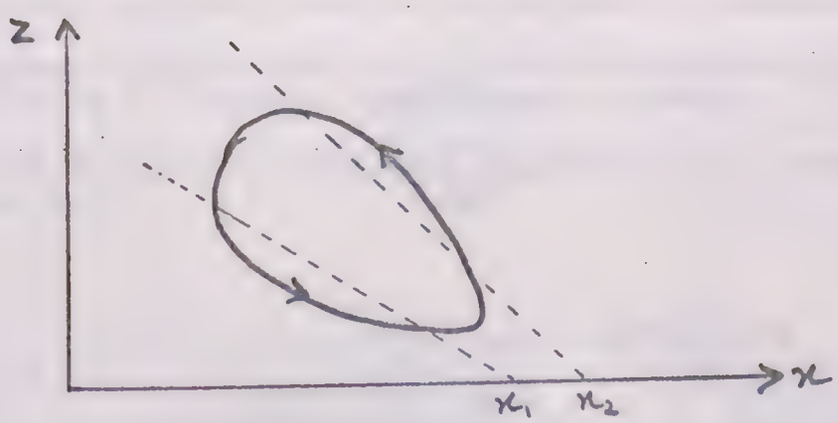

Fig 4c

In consequence there is strong vertical shear near the ground. The significance of this result is discussed below.

3. FRONTOGENESIS

A front delineates the boundary between two different airmasses. The position of this boundary is determined by the motion within the cyclones and anticyclones but the structure of the front itself depends on more local processses. This is well illustrated by the fact that global forecast models predict only the position of airmass boundaries and it is left to the forecaster to define the precise position and characteristics of the front. But why should frontal discontinuities develop? Why do certain parts of the polar front become active? (NB a baroclinic zone is <u>not</u> another term for a frontal zone).

There are several types of motion that have the property of tightening thermal gradients. The four most important are shown in Figure 5; (a) and (b) are for horizontal motion and (c) and (d) for vertical motions. Since fronts are formed in response to synoptic scale motions (ie mainly horizontal motion) it is to the horizontal deformation that we first look for frontogenetic effects.

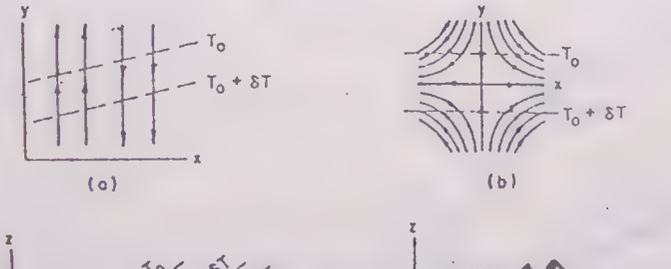

Figure 5. Four flow configurations which can intensify horizontal temperature gradients: (a) horizontal shear; (b) horizontal deformation; (c) vertical deformation; (d) differential vertical advection. (Adapted from Hoskins and Bretherton, 1972.)

Figure 6 shows a simplified baroclinic wave. It is taken from a numerical model specifically designed to study the development of such waves but the development is similar to that which occurs in the Meteorological Office forecast model. Shown on the diagram are regions of horizontal deformation (b) and horizontal shear between (a) and (a). It is in these regions that there tends to be a tightening of the thermal gradient and hence a local increase in the strength of the baroclinic zone.

A tightening thermal gradient means that $\partial\theta/\partial x$ is increasing. Since the front remains in thermal wind balance (F.13) this implies that $\partial v_g/\partial z$ is increasing, ie V_g is increasing and $dv_g/dt \neq 0$. From F.10 an ageostrophic motion, u' , is generated and, through F14, vertical motion w results. u' and w are linked through a streamfunction and, (F.22), the ageostrophic motion takes the form of a deformed ellipse Fig 7, the significance of the deformation being that the maximum vertical shear occurs near the ground. This, cf Fig 5d, concentrates the thermal gradient and reinforces the frontogenesis.

There is therefore a positive feedback mechanism which works like this:

i) Synoptic scale horizontal motion locally concentrates the isotherms.

ii) In these regions ageostrophic motion is generated.

iii) The ageostrophic motion produces differential advection which continues to increase the thermal gradient,

iv) which produces stronger ageostrophic motion, and so "ad infinitum".

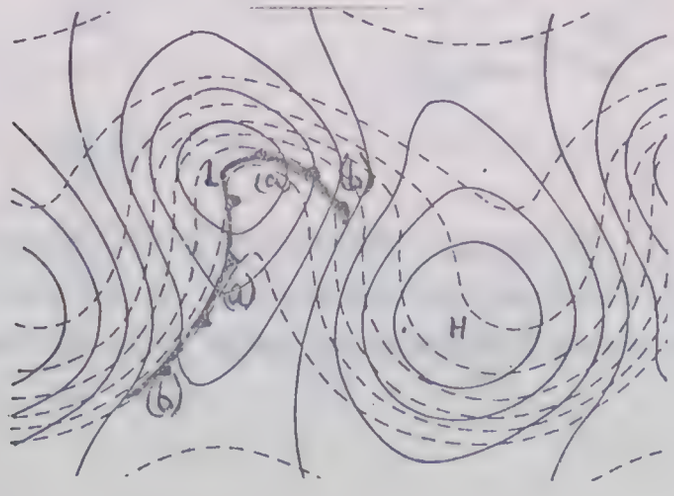

Figure 6. Dashed lines represent thermal thickness lines and solid lines the 1000mb contours. Depicted is a simplified baroclinic wave. (a) and (b) mark respectively areas of horizontal shear and deformation.

The process is finally showed by the effects of turbulent diffusion (internal friction). Another process, tending to destroy the temperature gradient, is the adiabatic cooling of the rising warm air and the warming of the sinking cold air.

Active frontal zones last for typically two or three days. What causes their dissipation? Referring back to the discussion of Figure 7 it will be recalled that the tightening of the thermal gradient resulted from the shape of the circulation, and this acts on time scales of 12-24 hrs. However the circulation has a secondary effect in that it also reduces the overall slope of the frontal zone. Refer to Margules formula $\tan\phi = f\bar{T}\Delta v / g\Delta T$. As ϕ decreases Δv decreases (note that ΔT is effectively horizontal temp gradient which also decreases as the slope decreases, so Δv decreases more rapidly) and the front decays. Since the atmosphere remains in approximate thermal wind balance an alternative way of visualising this is to observe that high momentum air from the upper level jet is advected downwards and low momentum air from the surface is advected upwards. The circulation destroys the thermal gradient and 'mixes' the momentum; ie the ageostrophic circulation eventually destroys the front. However this process of frontolysis takes much longer than that frontogenesis, hence quasi-steady-state fronts.

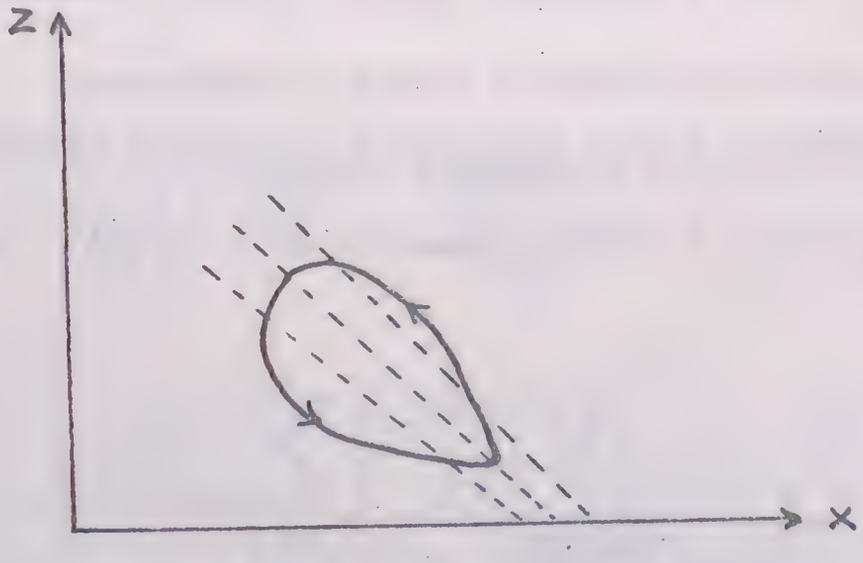

Figure 7. A model of the ageostrophic component of motion within a cold frontal zone. The x-axis is perpendicular to the surface front. Dashed lines denote θ surfaces and solid lines the local streamlines.

4. GEOMETRICAL INTERPRETATION OF FRONTS AND FRONTOGENESIS

4.1 Introduction

In Section 2 a scale analysis was presented for motion near frontal regions and solutions of the resulting simplified equations of motion were then discussed. It was shown how a positive feedback mechanism existed which meant that pre-existing temperature gradients were increased, and that on a larger time scale the slope of the frontal region was decreased, leading to a reduction in temperature gradient. A balance is thus established leading to quasi-steady-state fronts.

In this section we describe solutions of the equations derived in section 2 using geometrical arguments. These allow solutions to be obtained for simple initial data illustrating the effects described above. These arguments can also be used to explain other properties of atmospheric fronts.

These notes form a brief introduction only. A more detailed derivation is given in the attached reprint, which also contains a full list of references.

4.2 Method of Solution

The same notation is used as in section 2. (The notation is slightly different in Cullen (1983). Equation numbers preceded by F refer to section 2. We solve equations (F.10) to (F.15). For convenience we use the quantity defined before equation (F.24),

$$X = x + v_g/f$$

Making the assumptions that $v = v_g$ and

$$u = u_g + u' = -\frac{1}{f}\frac{\partial p}{\partial y} + u' \; ;$$

equation (F.10) becomes

$$\frac{dX}{dt} = u_g \qquad \text{(F.25)}$$

and equations (F.12, F.14 and F.15) give

$$\frac{d\theta}{dt} = 0 \qquad \text{(F.26)}$$

$$\frac{\partial u}{\partial x} + \frac{\partial w}{\partial z} = 0 \qquad \text{(F.27)}$$

$$\frac{d}{dt} = \frac{\partial}{\partial t} + u\frac{\partial}{\partial x} + w\frac{\partial}{\partial z} \qquad \text{(F.28)}$$

Consider a geometrical interpretation of these equations. As each fluid element moves, the rate of change of any property C of that element is dC/dt, with d/dt defined by (F.28). Therefore X changes only due to the geostrophic part of the wind, u_g, and θ is conserved. The continuity equation (F.27) means that the area of each element in the (x,z) plane is conserved. The remainder of the solution of the problem is given by (F.13), which gives

$$\frac{dx}{dz} = \frac{1}{f}\frac{\partial v_g}{\partial z} = \frac{g}{f^2\theta_0}\frac{\partial \theta}{\partial x} \qquad \text{(F.29)}$$

A simple idea of the type of solution obtained is given by considering two-dimensional cross-section of a frontal region and treating the initial data as piecewise constant (Fig.8). In each segment, θ and X are supposed to be uniform, with values θ_i and X_i as indicated. The slope of the line separating two segments is given by thermal wind balance (F.29) to be

$$S = \frac{\partial z}{\partial x} = \frac{f^2\theta_0}{g}\frac{[X]}{[\theta]} \qquad \text{(F.30)}$$

where [X] is the difference in X across the segment boundary. In the simple case of just two segments we obtain the Margules formula for the slope of the front.

Now consider the time evolution of the front. In section 2 it was shown that the first requirement is a geostrophic flow tending to concentrate the temperature gradients, for instance the deformation field shown in Fig 5(b). This can be written as

$$u_g = -\alpha x$$
$$v_g = \alpha y \qquad \text{(F.31)}$$

If this is substituted into the equations of motion, we obtain

$$\frac{dx}{dt} = -\alpha X \qquad \text{(F.32)}$$

$$\frac{d\theta}{dt} = 0$$

$$\frac{\partial u'}{\partial x} + \frac{\partial w}{\partial z} = 0, \quad \frac{\partial u}{\partial z} - \frac{\partial w}{\partial x} = -\alpha$$

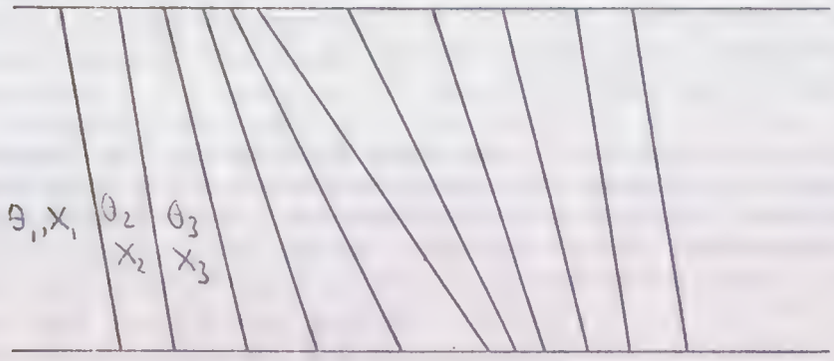

Figure 8

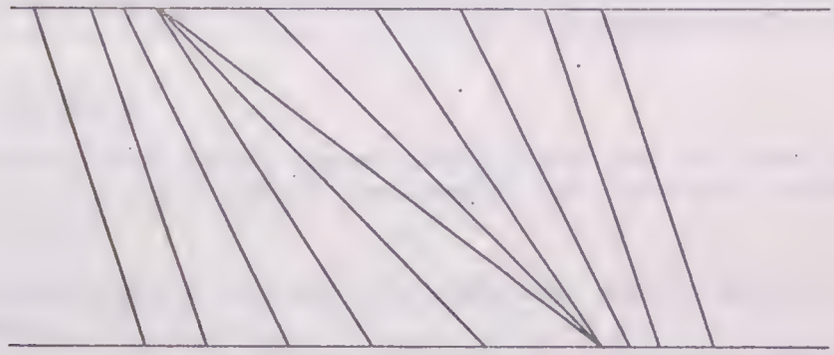

Figure 9

Figure 10

The system (F.32) states that, as time evolves, the value of X for each fluid particle is $X_0 e^{-\kappa t}$, where X_0 is the initial value. However, $\theta = \theta_0$ for all time. The area of each fluid element is proportional to $e^{-\kappa t}$. The slope of lines separating segments is proportional to $[X]$ which is proportional to $e^{-\kappa t}$. Thus the slopes reduce in time.

Starting with the initial data in Fig 8, the combined effect of the reducing slopes of the isotherms and the shrinking of the cross-section of the fluid elements is to produce a discontinuity at the boundary in a finite time (Fig 9). As the evolution continues, the temperature difference across the front increases. However, the front weakens rapidly away from the boundary and the solution remains continuous in the centre of the atmosphere (Fig 10). This is because of the frontolytic effect of the ageostrophic flow in this region discussed in section 2. The implied cross frontal circulation is sketched in Fig 11. In addition to the elliptical circulation shown in Fig 4, there is a minimum of vertical motion near the intersection of the frontal zone with the boundary.

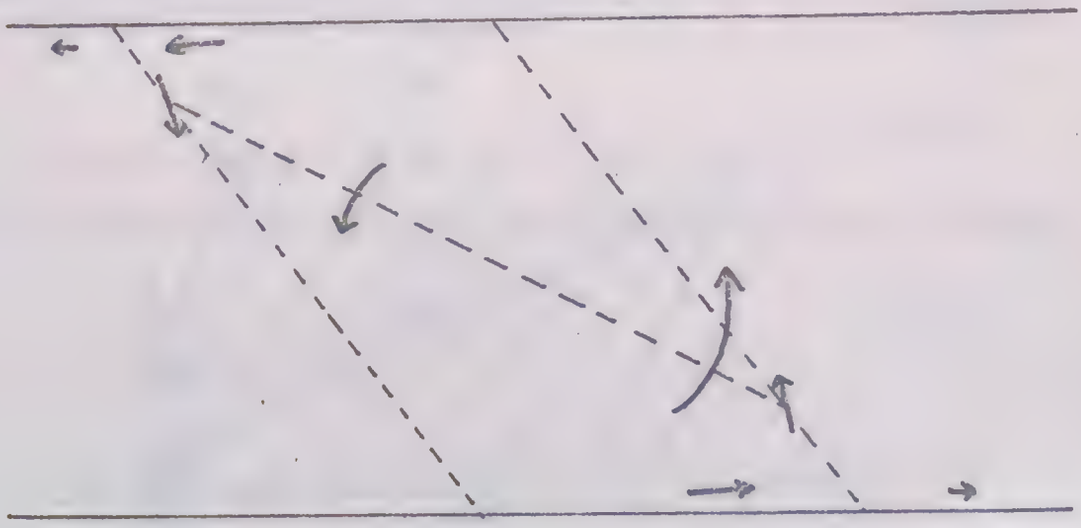

Figure 11.

4.3 Limitations of Model

The geometrical solutions that we have described provide a simple picture of how fronts evolve in the atmosphere, given large scale geostrophic flow which tends to concentrate gradients. As was discussed in section 2 and 3, the observed structure of fronts depends considerably on surface friction, as well as on the effects of latent heat release. Even without these effects, the idealisation of a front as a discontinuity is a considerable simplification. The real thickness will be limited by the onset of turbulence, which depends on the local Richardson number. In the model presented here this is proportional to

$$\frac{\partial \theta}{\partial z} \Big/ \left(\frac{\partial v}{\partial z}\right)^2 .$$

For fixed changes of v and θ across the front this is proportional to Δz, the frontal thickness. When it becomes less than 1/4 turbulent mixing sets in. In very stable conditions much sharper frontal zones are to be expected than in weakly stable conditions, because the jump in θ will be larger.

4.4 Further Results

The geometrical ideas described here can be used to prove other results about this idealised model of fronts. Some of these are listed below:

(a) Fronts cannot extend through the whole depth of the atmosphere.

(b) Frontogenesis is always initiated at the lower or upper boundary. Fronts cannot be generated at the tropopause (though strong gradients can be).

(c) Fronts can only be formed for a rather restricted range of values of θ and X. Thus the formation of sharp frontal zones is not as common as might be expected. For other data the gradients can be intensified but there is no tendency to generate a discontinuity.

Further details are given in Met O 11 Technical Note No 162.

5. THE STRUCTURE OF EXTRA-TROPICAL CYCLONES

Although the frontogenetic process described above is the principal mechanism by which frontal systems are generated, there are many other features which are frequently found associated with the fronts within extra-tropoical cyclones.

Figure 12 illustrates a typical developing wave depression. Shown are the cloud canopy, the precipitation area, surface isobars and Θ_w isotherms and the position of the upper level jet. These may all be obtained from synoptic scale observations. More detailed studies have however revealed important flows within the frontal system. These are generally referred to as the Warm Conveyor Belt (WCB) and the Cold Conveyor Belt (CCB).

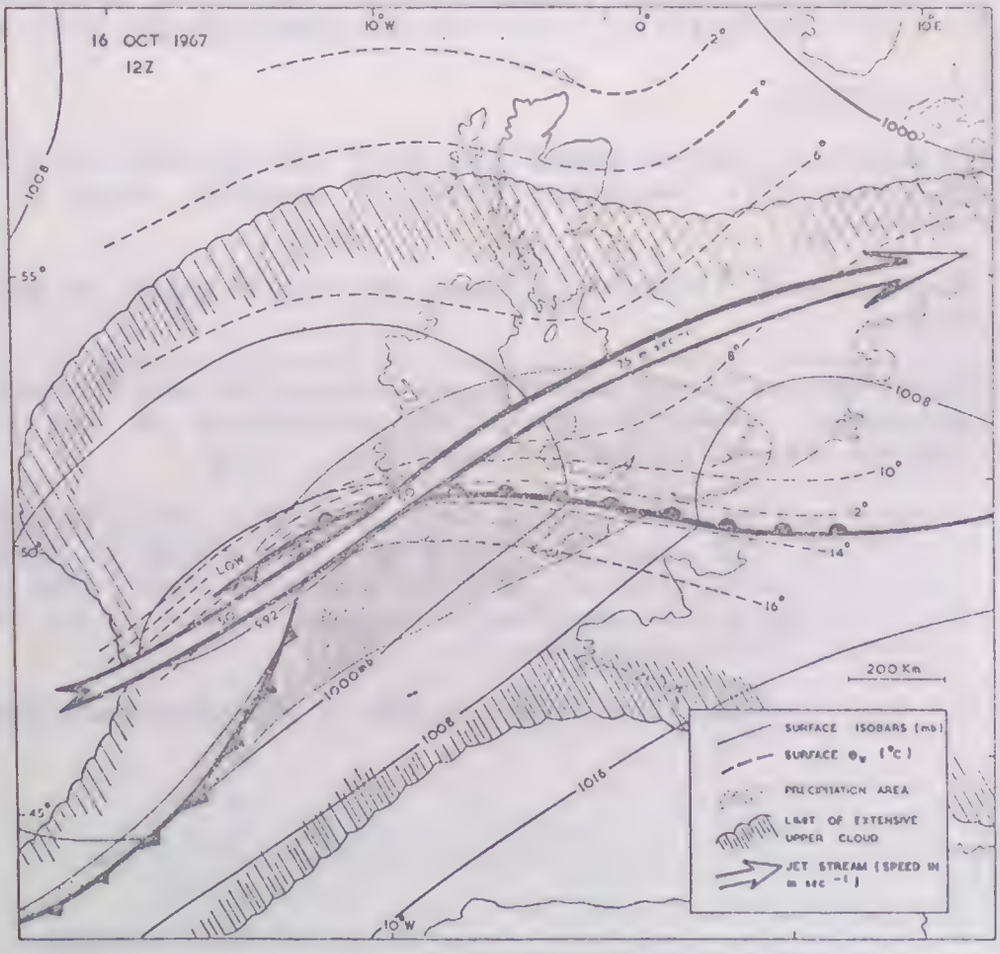

Figure 12. The structure of a typical open wave depression.
(from Browning and Harrold 1969)

a. The Warm Conveyor Belt

The WCB, illustrated in Figure 13 draws its air from the boundary layer in the warm sector. Warm moist air in this flow ascends at first gently as it moves parallel to the surface cold front and then more rapidly when it reaches the surface warm front and overrides the colder air. It rises well into the upper troposphere, turning anticyclonically as it does so, and is the principal cause of the extensive warm frontal cloud canopy. The convex-poleward boundary to this flow is often clearly marked on satellite visible imagery by the shadow it throws on the lower overcast. The cloud within the WCB flow eventually evaporates as it subsides in the NW'ly winds on the east flank of the ridge aloft.

b. The Cold Conveyor Belt

The other main cloud-producing flow is the CCB (Figure 14). This originates in the anticyclonic flow to the northeast of the cyclone and, relative to the advancing cyclone, it makes its way westwards just ahead of the surface warm front beneath the WCB. As it travels westwards it may rise a little beneath the WCB but its main ascent occurs after it emerges from beneath the western edge of the WCB. In rising it turns anticyclonically and merges, or folds beneath, the WCB. Carlson (1980) says this occurs if the cold air ahead of the warm front is warmer than that behind the cold front. Otherwise the CCB air may not rise but on emerging from beneath the WCB may turn cyclonically and sink.

Both conveyor belts are typically 200 km wide and, away from the centre of the cyclone some 1-2 km deep. As they rise the moisture condenses and they produce deep cloud systems. Together they give rise to the characteristic large comma-shaped cloud pattern seen in satellite imagery.

The cloud is deepest and the precipitation is at its heaviest near the apex or triple point of the system.

The conveyor belts are separate entities and can, and often do, exist on their own. Of the two, the WCB is more important in terms of forecasting as, coming from the south, it carries most of the moisture and hence dominates the precipitation forming characteristics of the system. The WCB can take many configurations, which lead to different frontal structures, but conceptually it is helpful to think in terms of two archetypal models. These are illustrated in Figure 15 which showsthe rearward sloping ascent model and the forward sloping ascent model. In the case of rearward sloping ascent, the WCB rises with a component of relative flow towards the cold front. (Figure 15b). In the more common situation of forward sloping ascent the WCB ascends with a component of relative flow towards the cold front. (Figure 15 b). In simple terms the former corresponds to situations in which most of the activity is in the vicinity of a well-defined cold front; the latter corresponds to situations in which most of the activity is in the vicinity of a warm frontal zone. However, there are other variations, see for example the split cold front described by Browning and Monk (1982).

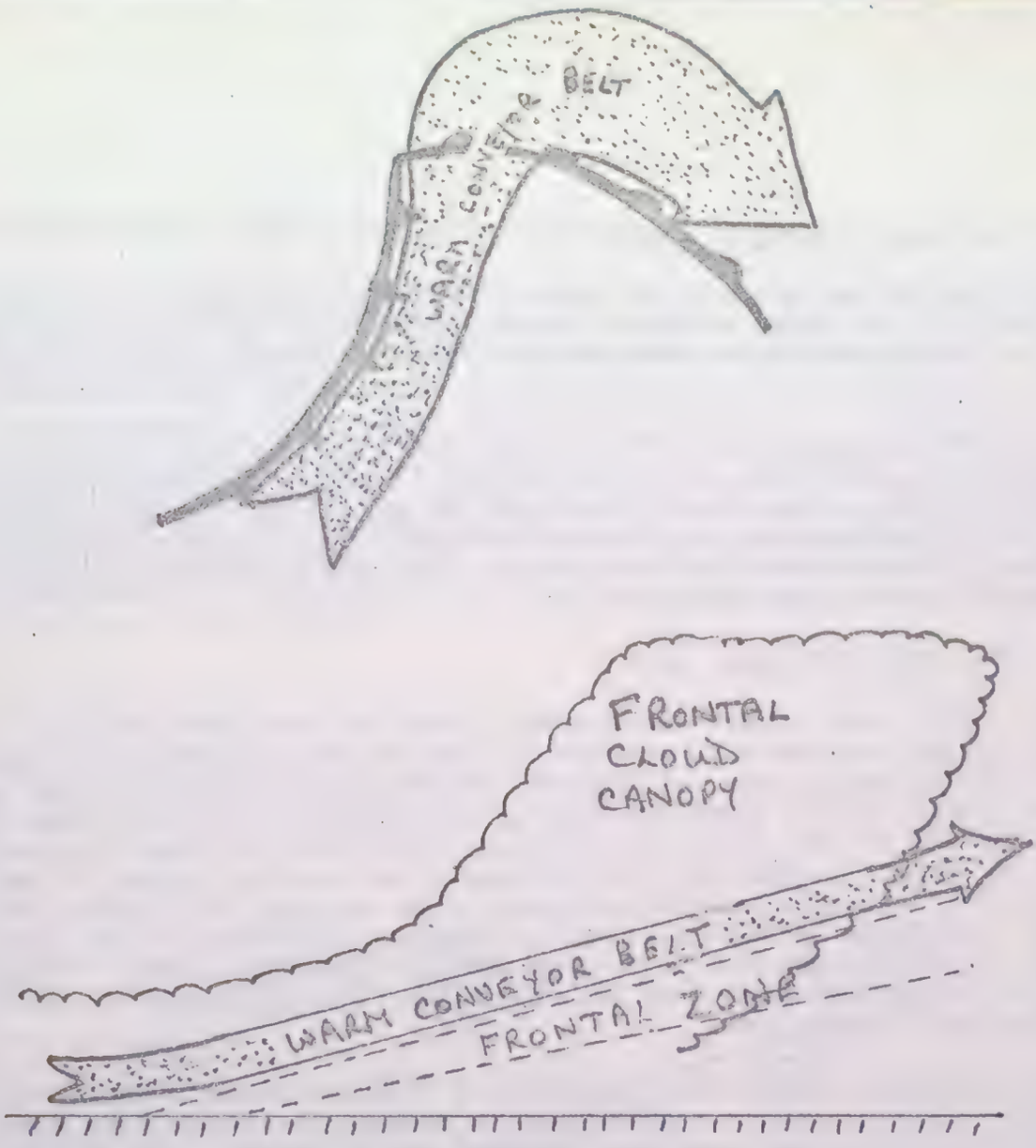

Figure 13. Schematic diagram of the warm conveyor belt.

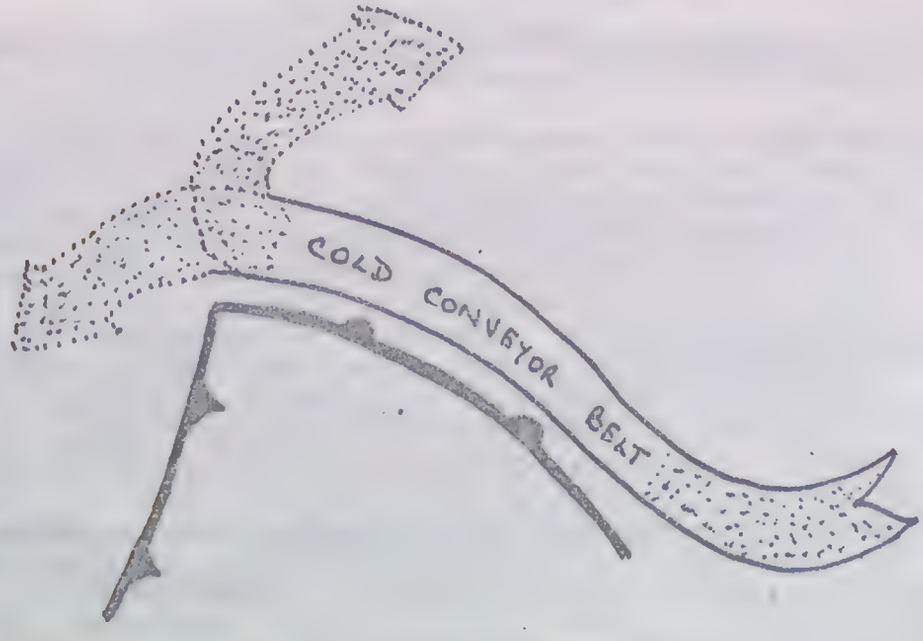

Figure 14. Schematic diagram of the cold conveyor belt.

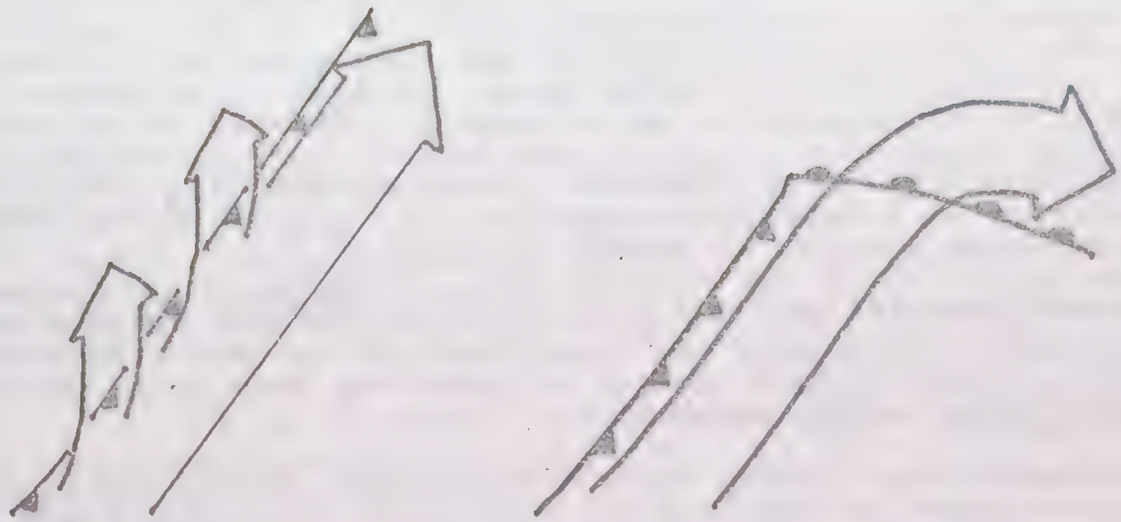

(a) (b)

Figure 15. Warm conveyor belt in relation to the surface fronts in the case
a) rearward sloping ascent
b) forward sloping ascent.

6. MESOSCALE INSTABILITIES (THEORY)

The concept of the Warm Conveyor Belt ascending above the warm frontal zone, Figure 13, gives the impression of uniform ascent. In consequence it may be supposed that the precipitation falling from frontal regions would also be uniform. However this supposition is false and in fact precipitation is usually produced on scales much smaller than those of the cyclonic and frontal circulations; on scales smaller than the WCB. Recent research has shown that the precipitation has a mesoscale organisation, usually in the form of bands orientated parallel to one of the frontal zones. Figure 16 is a schematic depiction of the various types of mesoscale rainbands that have been observed. Not all occur in every frontal system, indeed some systems exhibit none and have relative uniform precipitation everywhere. However, each type of rainband has been seen, and can be expected to occur fairly frequently.

Since air above the frontal zone is saturated, the rainbands may be seen as evidence of regions of ascending air within the mid-troposphere, ie the rainbands are the visible evidence of mesoscale instabilities embedded in the frontal zone.

The remainder of this section discusses the theory of some of these mesoscale instabilities. For others no satisfactory theory yet exists. Which theory is relevant to which type of rainband will be indicated in the next section.

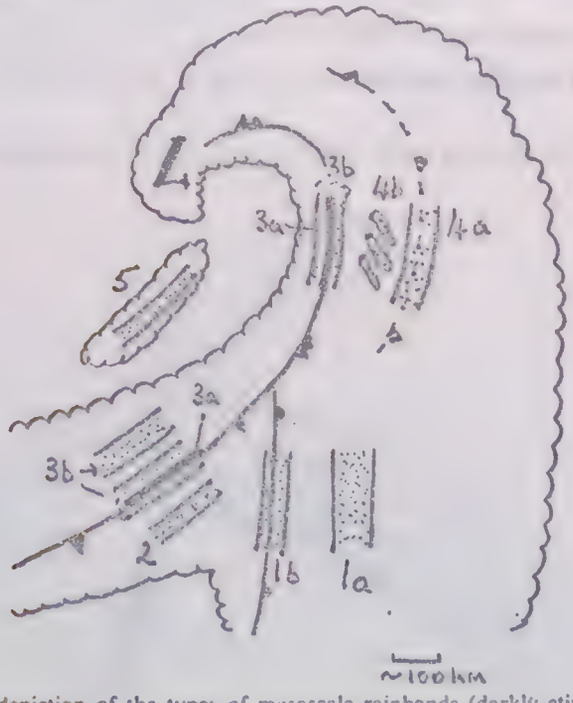

Figure 16 Schematic depiction of the types of mesoscale rainbands (darkly stippled areas) observed in extratropical cyclones. The upper-level cloud shield of the cyclone is shown.

Type 1: Warm frontal rainbands, of which type 1a occurs ahead of and parallel to the surface warm front, while type 1b coincides with the surface warm front. Type 2: Warm sector rainbands, which occur parallel to and ahead of the surface cold front. Type 3: Cold frontal rainbands, of which type 3a is very narrow and coincides with the cold frontal passage, while type 3b is wider and may straddle the narrow cold frontal rainband or lag behind it. Type 4: The surge rainband, type 4a, coincides with the leading edge of a surge of cold air aloft, ahead of the main cold front in the occluded portion of the cyclone. A field of convection, frequently organized in small rainbands, type 4b, occurs behind the surge rainband. Type 5: Postfrontal rainbands, which occur in the cold air mass to the rear of and parallel to the cold front and usually to the rear of the large cirrus shield associated with the cyclone.

The vorticity (ξ) of a fluid parcel at rest on the surface of the earth is f. . However near a front (considered as a two-dimensional phenomenon), see Figure 17, it has extra vorticity due to the wind shear.

$$\xi_a = f + \frac{\partial v}{\partial x}$$

and ξ_a is referred to as the absolute vorticity. Integrate with respect to x

$$\int \xi_a \, dx = fx + v \, .$$

$\int \xi_a dx$ is the absolute momentum of a fluid parcel and often labelled M ie.

$$\underline{M = fx + v} \qquad \left(\text{note } \frac{dM}{dx} = f + \frac{dv}{dx} = \xi_a\right)$$

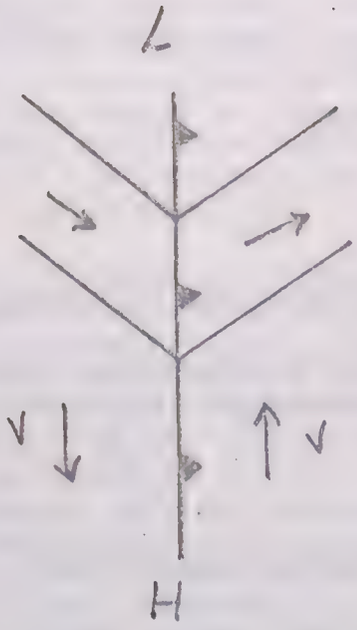

Figure 17. Absolute vorticity of a fluid particle is

$$\xi_a = f + \frac{\partial v}{\partial x}$$

Note that for a two dimensional front there is no variation of u with y and so $\frac{\partial u}{\partial y} = 0$.

Differentiate w.r.t time

$$\frac{dM}{dt} = f\frac{dx}{dt} + \frac{dv}{dt}$$

$$\text{or} \quad \frac{dM}{dt} = fu + \frac{dv}{dt} \qquad \left(u = \frac{dx}{dt}\right)$$

Now relate this to the equations of motion of a fluid which are

$$\frac{du}{dt} - fv = -\frac{1}{\rho}\frac{\partial p}{\partial x}$$

$$\frac{dv}{dt} + fu = -\frac{1}{\rho}\frac{\partial p}{\partial y}$$

In the special case of a flow which is independent of y, ie two dimensional motion in the (x,z) plane and considering motion relative to the front (moving at speed u).

$$\frac{dv}{dt} + fu = 0$$

and so

$$\frac{dM}{dt} \equiv 0$$

showing that M is a conserved quantity following the motion.

It is also well known that in the absence of latent heat release (ie a dry atmosphere), potential temperature is conserved.

$$\frac{d\theta}{dt} = 0$$

In a saturated atmosphere this must be written

$$\frac{d\theta_w}{dt} = 0$$

In a moist atmosphere it is better to take $\frac{d\theta_v}{dt} = 0$ where θ_v is the virtual potential temperature.

For two dimensional flow in a moist atmosphere (neglecting rain) the two quantities M and θ_w are conserved. In consequence whenever a parcel of air is displaced, a restoring force is generated which tries to restore the parcel to its equilibrium surface. Consider Figure 18 which depicts an air-tube (two dimensional flow) initially at rest at z=o with its axis parallel to the y-axis. Let M and θ_v denote isopleths of these two quantities within the environment and the particular surfaces have been chosen to intersect with the tube at z=o. If the tube is displaced to a point A, it will be

a) colder than its environment and sink back to

b) have lower momentum than its environment and move horizontally back to M.

The resultant forces will act to return the tube to its original position. By a similar reasoning a displacement to point C will result in an upward and westward unstable acceleration. Points B and D as well as the initial point are equilibrium positions; point D and the initial point represent stable equilibria while point B is an unstable equilibrium position. Compare Figure 18, and the above discussion, with convection and a tephigram the M surface corresponds to the environmental curve and the θ_v surface the ascent path of a parcel of air. We may continue the analogy by defining the'Slantwise Convectively Available Potential Energy' (SCAPE) as the potential energy released during ascent and define it in an analogous way to the Convectively Available Potential Energy (CAPE) which is so useful in quantifying the energy available for convective processes. However do not think of this new 2-d instability as having the physical form of convective clouds. Its nature will be discussed later.

The above theoretical ideas are illustrated in Figure 19 which is a cross-section perpendicular to an active cold front which crossed the British Isles on 13 January 1983. Depicted are isopleths of θ_w, which in a saturated atmosphere are parallel to θ_v, and isopleths of $M = fx + V$ where V is the component of velocity parallel to the front. The lower part of the upper tropospher jet is visible at (50 km, 450 mb) and the field of $M(= fx + V)$ is not dissimilar from the more familiar V-field. Notice particularly that θ_w and M surfaces are almost parallel in the frontal zone indicating that a parcel ascending the front can conserve both quantities simultaneously: a feature that would be expected in a 2-dimensional frontal zone. However there are regions where θ_w and M surfaces cross, indicating that parcels of air cannot conserve both quantities ie ageostrophic flow is present. Consider a tube of air at O' which is displaced to A'. By reference to Figure 18 it will be seen that there is a restoring force at A' and hence within parts of the frontal zone there is stability. However, above the frontal zone (O,A,B,C,D) there is stability at A but instability at C.

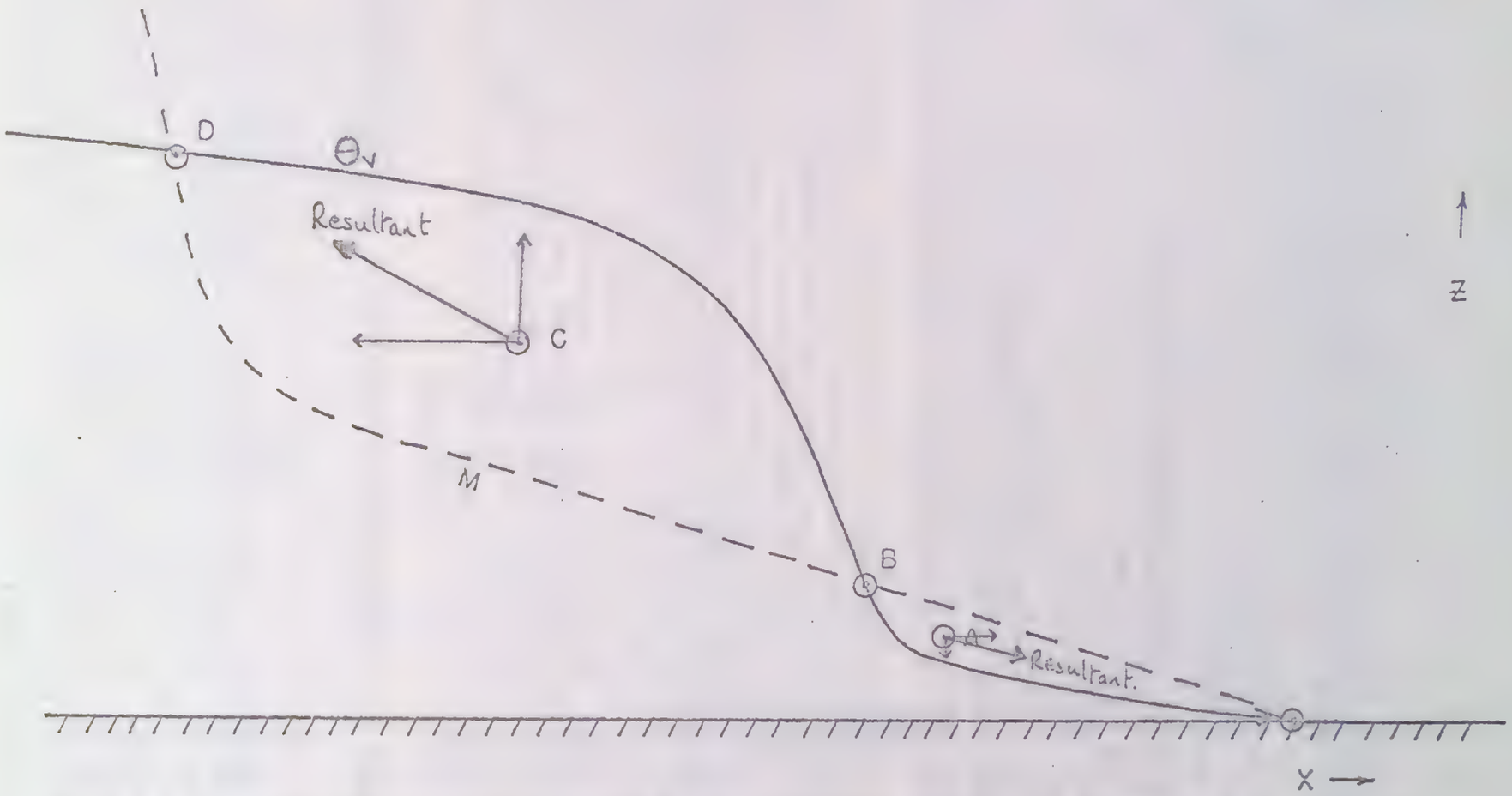

Figure 18. Instability generated when parcels are displaced from M or Θ_V surfaces. Note that the force due to changes in M acts along geopotential surfaces and that due to changes of Θ_V acts in the vertical as it is basically buoyancy.

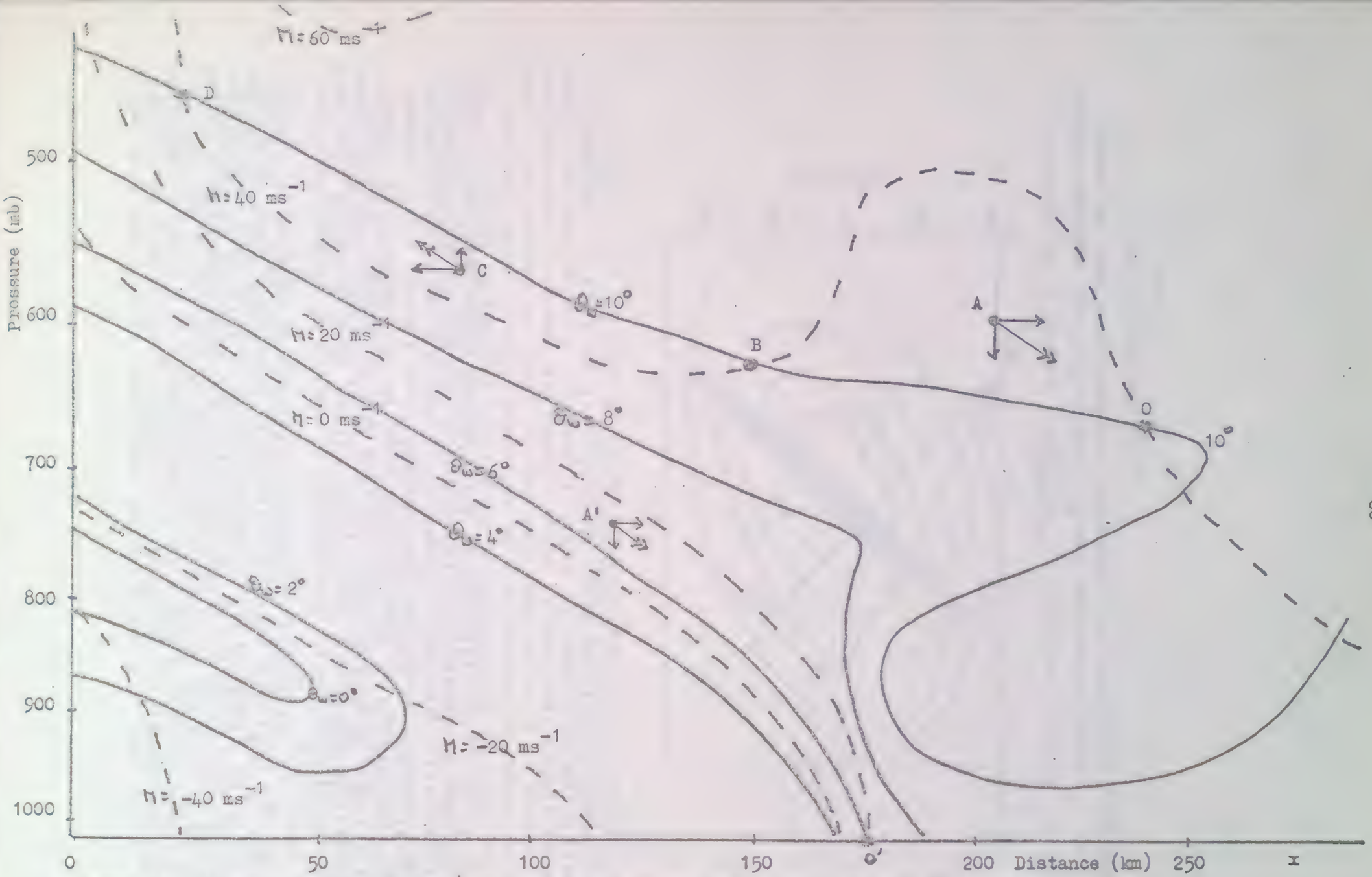

Figure 19. 13 January 1983. Cross-section of a cold front showing isopleths of θ_ω (solid lines) and M (=fx+v) (dashed lines). For furthur details see text.

The question now is "what does this instability look like?" Firstly it is two dimensional, since it only develops in the absence of $\partial f/\partial y$. Secondly it is a perturbation on the normal frontal flow, with the energy being released in regions aligned with the frontal surface. In consequence it takes the form of a 2-dimensional roll perturbation with the axis of the roll aligned approximately parallel to the surface front, or, more precisely, aligned parallel to the thermal wind. An example of the roll is shown in Figure 20.

The instability is sometimes referred to as 'slantwise convection', 'slantwise' because of its inclination to the horizontal and 'convection' because of the analogy (described in Figure 18) with the CAPE. An alternative and more precise name is 'Conditional Symmetric Instability', 'Conditional' because the development depends on latent heat release (θ_w-surfaces), 'Symmetric' because historically this form of instability is 2-dimensional, ie symmetric about one of the axes. The wavelength of the rolls is typically 50-200 km.

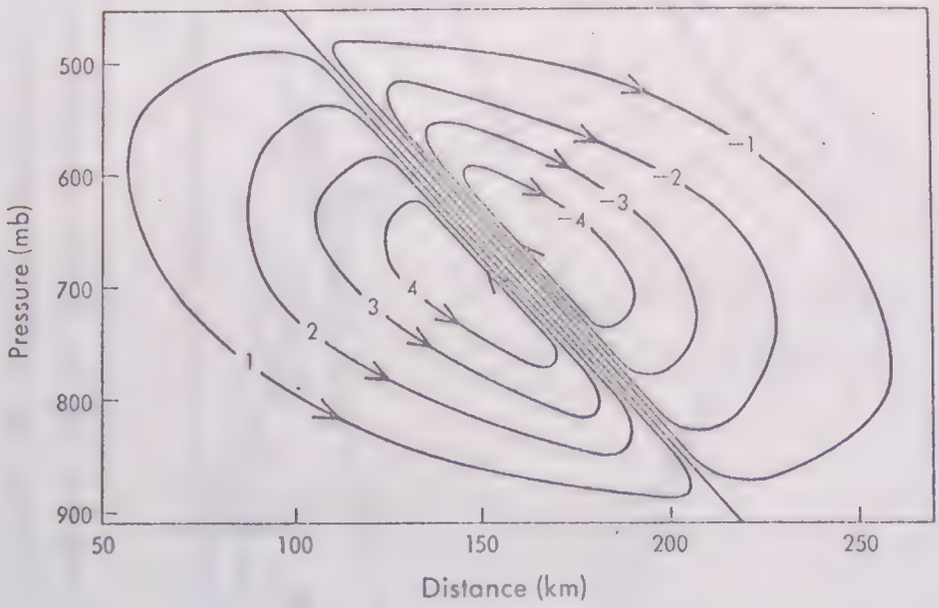

Figure 20. Conditional Symmetric Instability. The streamlines intervals are in arbitrary units.

To summarise this section we will consider the lifecycle of a parcel of air embedded within the warm conveyor belt. Originally, when the air is well south of the frontal zones it is fairly dry and vertical motion is weak ie θ is conserved. Since almost everywhere in the atmosphere θ surfaces are more shallow than M surfaces (see Figure 21) there is stability. However as the parcel approaches the frontal zones it is lifted up and becomes saturated. From then on the atmosphere conserves θ_w and (see Figure 19) θ_w surfaces are often steeper than M surfaces. The atmosphere therefore becomes unstable to slantwise convection and roll perturbations develop within the warm conveyor belt. Figure 22 shows how the vertical velocity field within the WCB is modified by the instability and therefore how the precipitation may be organised into bands.

There is one further property of the roll instability and that is its ability to generate differential advection, so that after a few hours the θ_w surfaces are overturned in certain regions of the roll. This leads to classical convection in preferred linear (since the roll is 2-D) regions or in more familiar terms, lines of convective clouds embedded within the frontal zone. These are commonly observed, but not predicted by classical frontal theory. The convective clouds enhance the rainfall as shown at the points marked X in Figure 22c, and emphasise the already slightly banded nature of the rainfall.

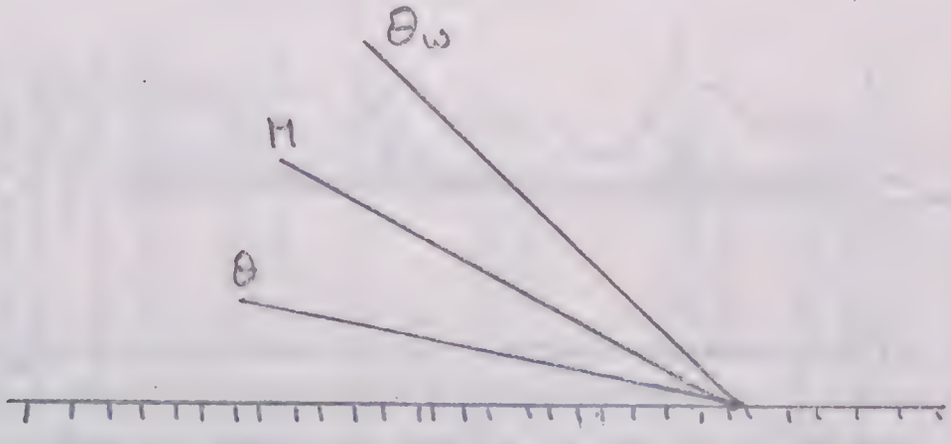

Figure 21. Relative inclination of θ, θ_w and M surfaces to the horizontal. Typical values range from $\theta \sim 1:150$ to $\theta_w \sim 1:25$, sometimes steeper.

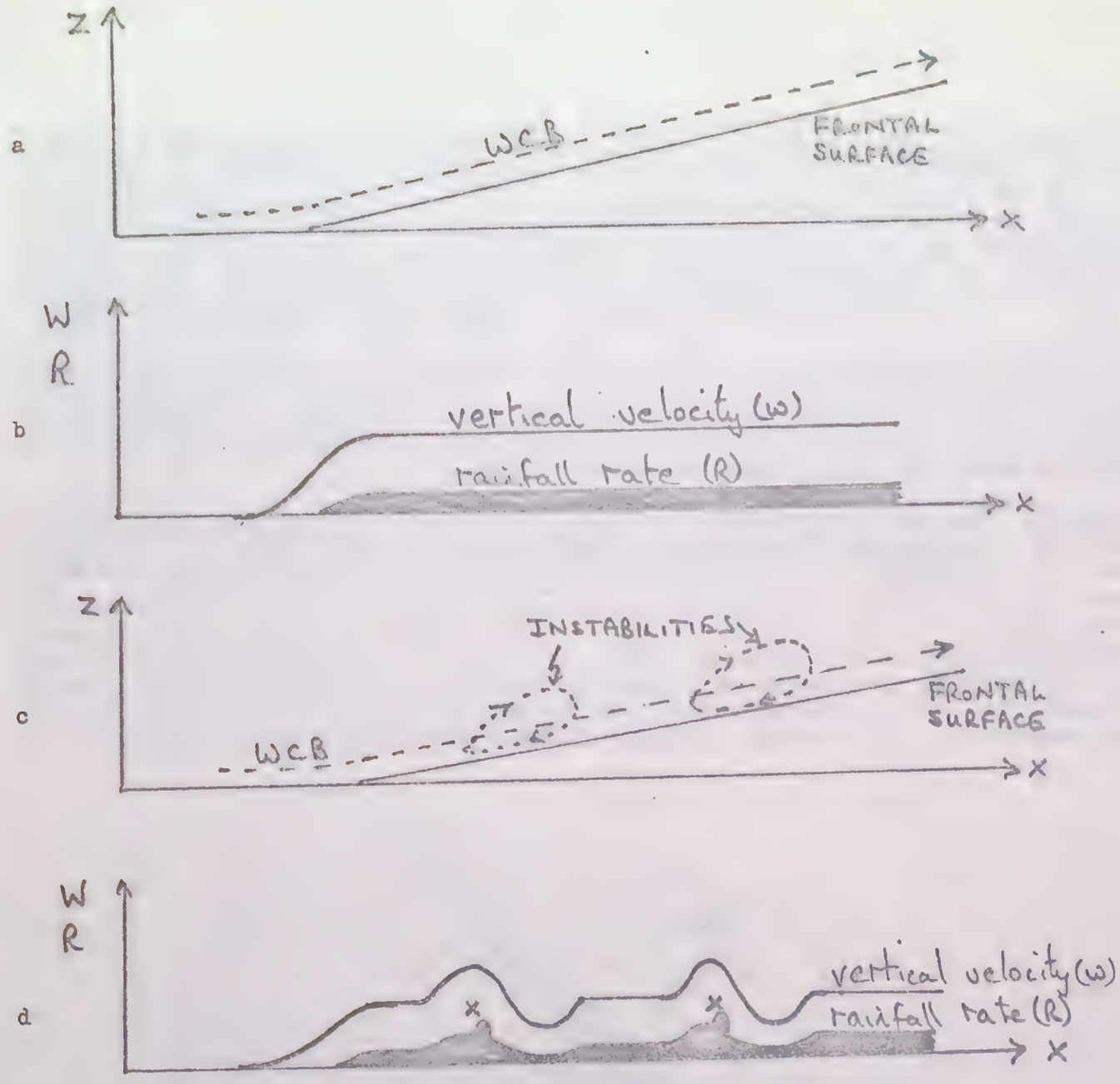

Figure 22. a) is a schematic diagram of the WCB ascending over the frontal zone. b) the vertical velocity experienced by a parcel of air embedded in the WCB. c) the WCB with embedded instabilities. d) the vertical velocity modified by conditional symmetric instabilities. Shaded areas give a qualitative idea of rainfall. The relevance of the points marked X in (d) is discussed in the text.

Figure 23. Classification of mesoscale rainbands

Broad classification		Detailed Classification (after Hobbs 1978) No.	Name	Width*	Frontal† archetype into which associated	Location and orientation	Some published examples
U-type	Upper or middle tropospheric convective rainbands	1	Warm frontal rainband	W	FSA	Parallel to the warm front and either on or ahead of it	Browning and Harrold, 1969 Herzegh and Hobbs, 1978a Heymsfield, 1979
		4a	Pre-frontal cold surge rainband	W	FSA	Parallel to and just ahead of an overrunning upper cold front	Kreitzberg, 1964 Kreitzberg and Brown, 1970 Browning et al, 1973
		3b	Cold frontal rainband	W	RSA	Parallel to and either behind or straddling an active surface cold front	Browning and Harrold, 1970 Hobbs et al, 1978
L-type	Lower tropospheric convective rainbands	3a	Narrow cold-frontal rainband	NN	RSA	Associated with line convection along a sharp surface cold front	Browning and Harrold, 1970 Browning and Pardoe, 1973 Hobbs and Biswas, 1979 James and Browning, 1979 Carbone, 1982 Hobbs and Persson, 1982
		4b	Small rainband (transverse)	N	FSA	Behind a cold surge rainband; perpendicular to winds	Matejka et al, 1980
			Small rainband Ø (longitudinal)	N	either?	Within a warm sector; parallel to winds.	Browning and Bryant, 1975
D-type	Deep convective rainbands	2	Warm sector rainband	W	either?	Ahead of and parallel to the surface cold front	Nozumi and Arakawa, 1968 Herzegh and Hobbs, 1978b
		5	Postfrontal rainband	W	either?	Behind the cirrus shield and parallel to the main cold front.	Houze et al, 1976

* W = wide (~50 km)
N = narrow (~10 km)
NN = very narrow line elements (<5 km)

† FSA = Forward sloping ascent
RSA = Rearward sloping ascent (see Section 4)

Ø This category not in Hobbs' classification.

7. MESOSCALE INSTABILITIES (OBSERVATIONS)

The remainder of the paper discusses the various types of bands depicted in Figure 16 and summarised in Figure 23.

a) Warm frontal rainbands type 1a and 1b

Warm frontal rainbands are typically 50-100 km wide. They are orientated parallel to the warm front and situated on or ahead of the surface warm front. A typical example is shown in Figure 24a and a schematic representation of the frontal motion associated with them is given in Figure 25 (after Browning et al 1973). The bands are usually associated with proturbances above the warm conveyor belt with the heaviest rainfall occurring below lines of mid-level convection within the warm front.

The model described in section 6 well fits these bands.

b) Warm sector rainbands

These are typically 50 km wide and orientated parallel to the cold front. An example is shown in Figure 26. Sometimes these warm sector bands move at the same speed as the cold front, ie are embedded in the flow in a similar manner to type 1, in this case they are generally weak and have a similar structure to type 1 bands. On other occasions they are composed of deep convective clouds (and are better described as a squall line as they can be quite vigorous) and propagate ahead of the cold front at 10-20 knots. (The detailed structure of squall lines will be dealt with in the notes on convective storms). In both cases however, there is a form of roll circulation and the presence of line convection but they may be distinguished on the basis of the nature of the rainfall (predominantly frontal or convective) and by whether the bands propagate with respect to the cold front.

c) Wide Cold Frontal bands, Type 3b

These bands are typically 50 km wide, orientated parallel to the cold front and situated on or behind the surface cold front. An example is shown in Figure 27 which is the rainfall associated with the front shown in Figure 19 (point C). In nearly all respects the bands marked are similar to Type 1 rainbands except that, as might be expected, the embedded convection tends to be slightly stronger. The band marked N is described below.

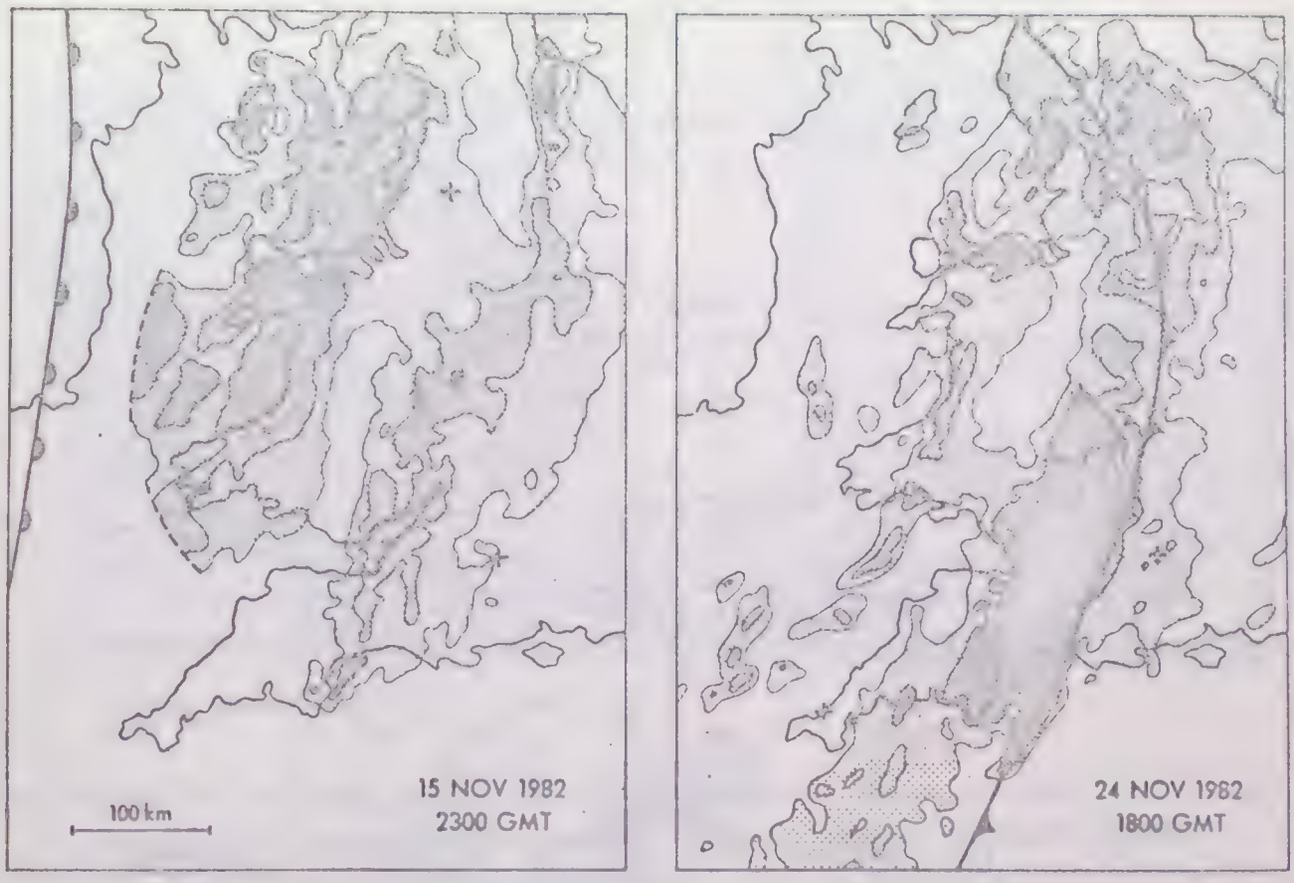

Figure24 Examples of rainbands observed by the UK weather radar network. (a) shows two very wide warm frontal rainbands. (b) shows two wide cold frontal rainbands (with a narrow cold frontal rainband embedded within one of them). Radar echo corresponding approximately to light, moderate and heavy rainfall intensities, respectively, is shown by light, moderate and heavy stippled shading.

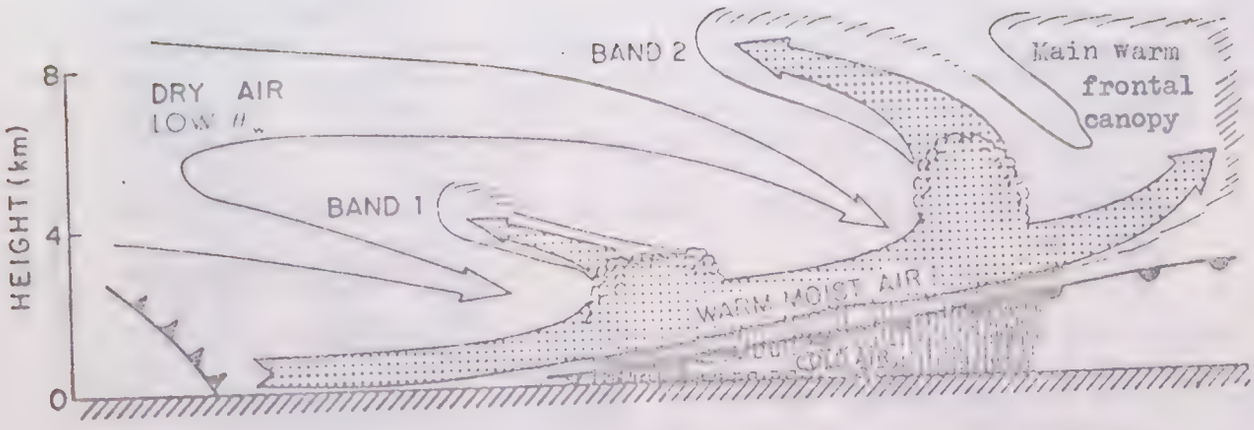

Figure 25 . Schematic cross section showing the airflow (relative to the system) within a mature frontal system. Warm conveyor belt air is undergoing forward sloping ascent above the warm frontal zone. However, air which ascends convectively at the top of the conveyor belt undergoes rearward sloping ascent within cloud canopies associated with individual cold surges aloft. (From Browning et al, 1973, as adapted by Wallace and Hobbs, 1977).

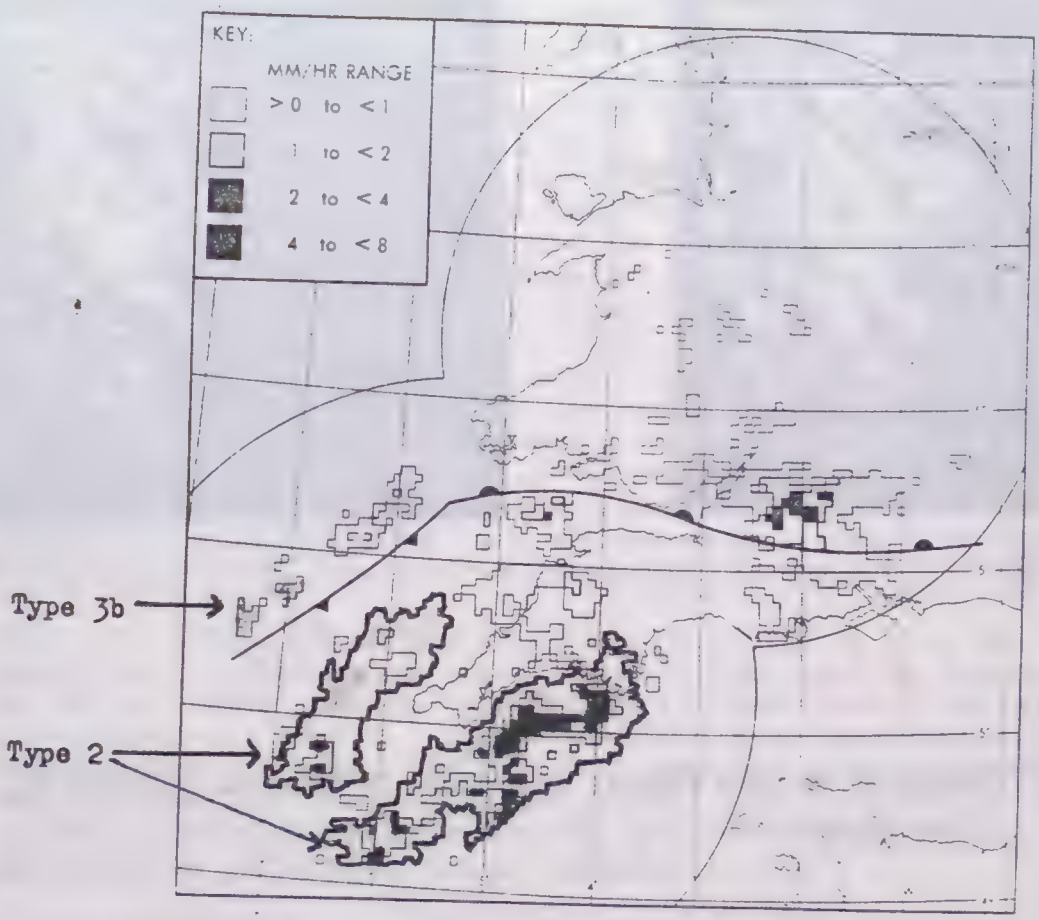

Figure 26 Rainfall distribution as shown by the United Kingdom radar network at 00GMT 29/07/79. Frontal positions have been superimposed

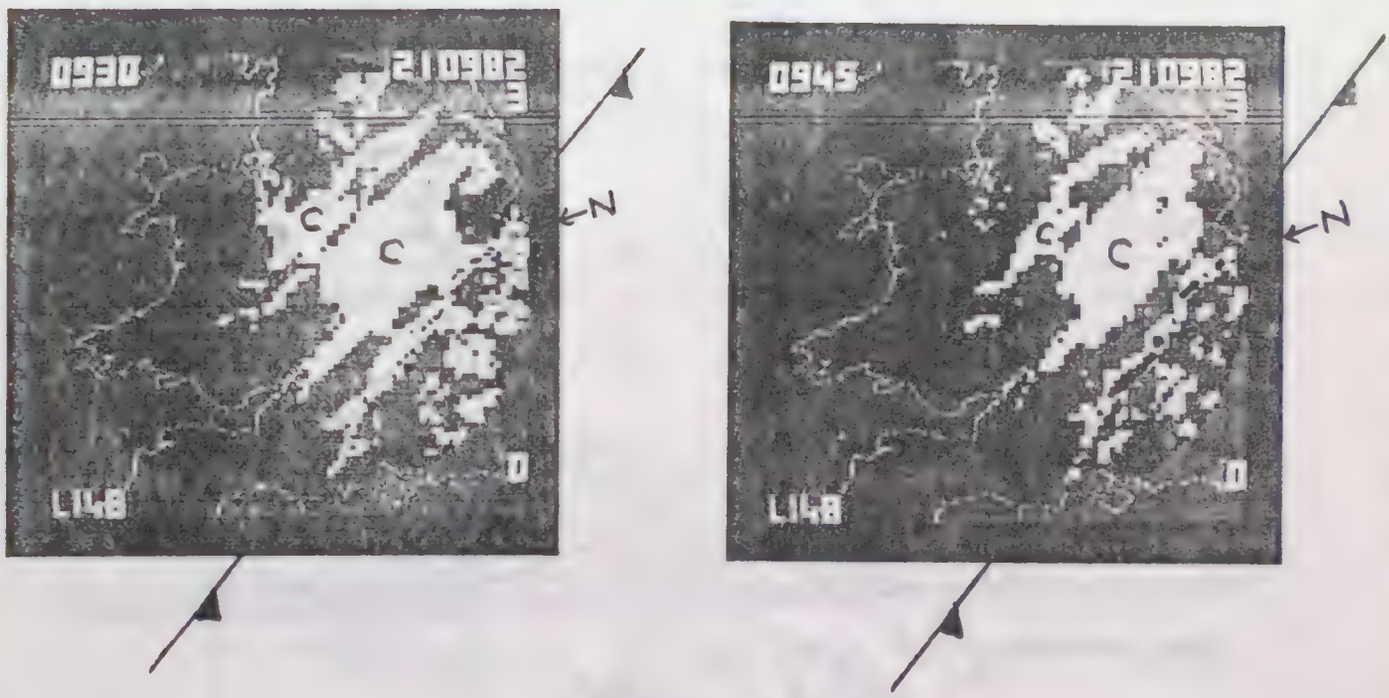

Figure 27. Examples of cold frontal rainbands. C= Type 3b. N = Type 3a.
(see Figure 16)

d) Narrow Cold Frontal Rainband, Type 3a

Narrow cold front rainbands are typically 3-5 km wide and coincident with the surface cold front. They are different in character to the previous types discussed and may best be considered as forced line convection. A schematic model of the airflow associated with Type 3a is shown in Figure 28.

The low level jet ahead of the surface cold front is the WCB discussed earlier, and the high level jet, the more well-known upper troposphere jet stream. Both jets are flowing northwards into the paper. Air within the frictionally backed lower portion of the low level jet is forced to rise abruptly to form a region of ascent which morphologically resembles a cliff edge. Air rises rapidly up the cliff face, subsides a little at the top, with some flowing forward over the top of the jet, but most flowing rearwards where it soon begins ascending again above the wedge of cold air coming in behind the surface cold front. Occasionally the cliff edge is undistorted and the line convection is undistorted over long distances (see Figure 29), and sometimes it is convoluted such that the line convection is broken into a series of line elements each $\sim$ 10 km in length and slightly backed from the orientation of the surface cold front.

The line convection manifests itself as a very narow band of heavy rain, often with small hail. The band is sometimes only 3 km wide, with sharp boundaries, and has a characteristic appearance on radar. Bands of this type are shallow features, located mainly below 700 mb, but they are often embedded within a deeper area of light-to-moderate, precipitation (ie Type 3b bands). This usually prevents the line convection from being detected in satellite cloud imagery.

e. Prefrontal cold surge rainbands, Type 4a

These bands are typically 50 km wide and are parallel to and situated just ahead of an over-running upper cold front (see Figure 16). They are similar in many respects to Types 1 and 3b bands.

f. Smaller rainbands, Type 4b

These rather insignificant rainbands may, on occasions, be seen behind a cold surge rainband. They are typically 10 km wide and orientated perpendicular to the winds. To distinguish them from other types of bands they are usually referred to as small rainbands (transverse). Small rainbands (longitudinal), not marked in figure 16 have the same width but occur in the warm sector and are parallel to the warm sector low level winds. This latter type appear to be formed by longitudinal rolls along the wind and occur within the boundary layer and its capping Sc layer. The cause of the transverse bands is, at present, obscure.

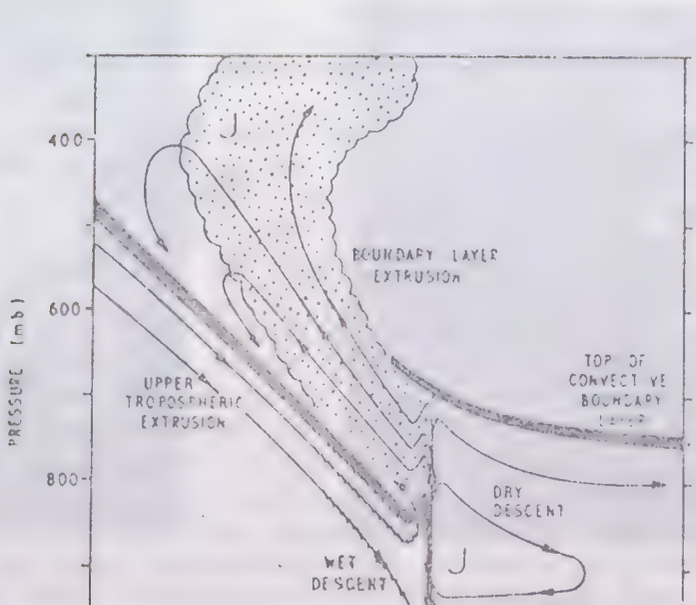

Figure 28. Schematic depiction of the airflow pattern transverse to a sharp cold front, illustrative of the rearward sloping ascent model. Thin lines are streamlines relative to the system. The letter J indicates the position of the upper tropospheric jet and the low-level jet in the warm conveyor belt, the main wind components of which are directed into the plane of the paper. Thick lines represent the cold frontal zone and the top of the convective boundary layer. The region of rearward sloping ascent is stippled. Relative humidity is high in the convective boundary layer ahead of the surface cold front (ie within the WCB) and this air becomes saturated when it is extr[illegible]ove the cold frontal zone. Air descending beneath the frontal [illegible]ne is initially dry but becomes more nearly saturated after [illegible]ering the region where precipitation falls into it. (From Browning and Pardoe, 1973).

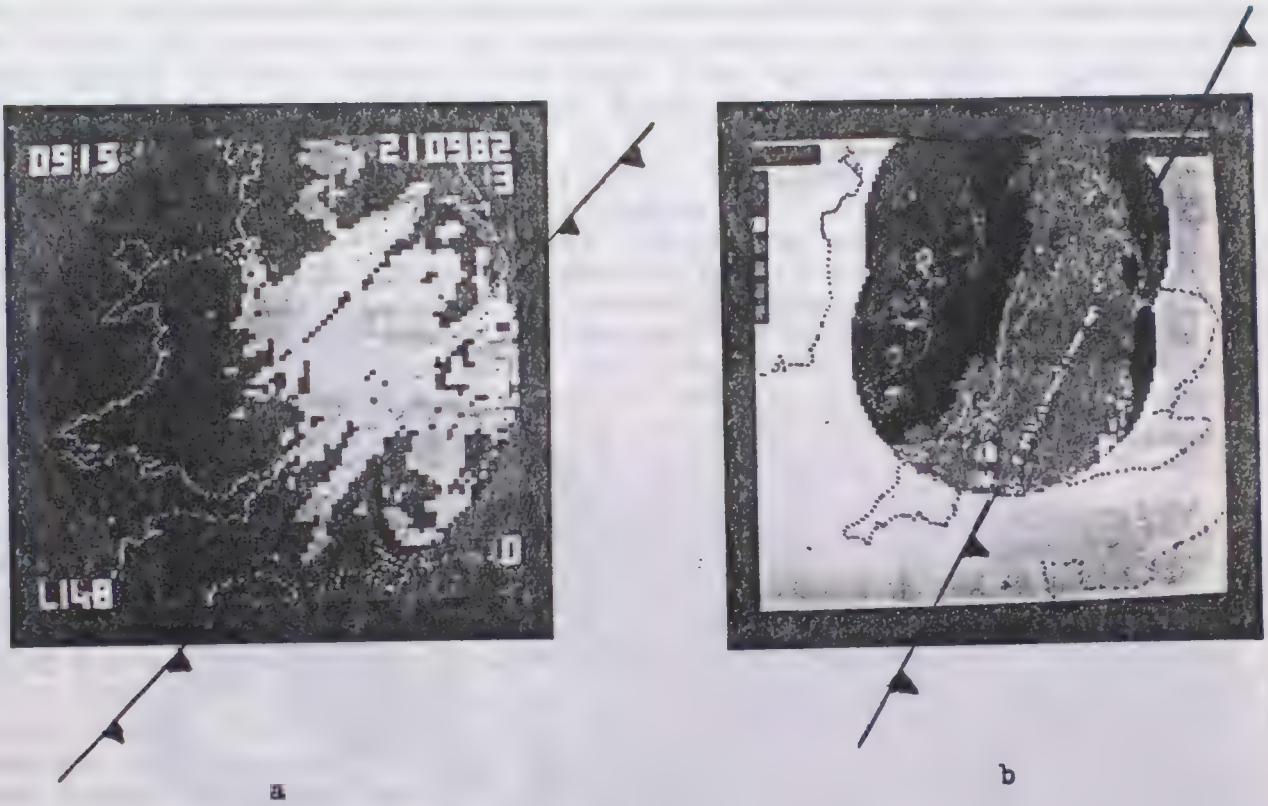

Figure 29. Examples of narrow cold frontal bands.

a) Distorted and broken in to line elements.

b) Undistorted and unbroken over long distances.
This is represented schematically below.

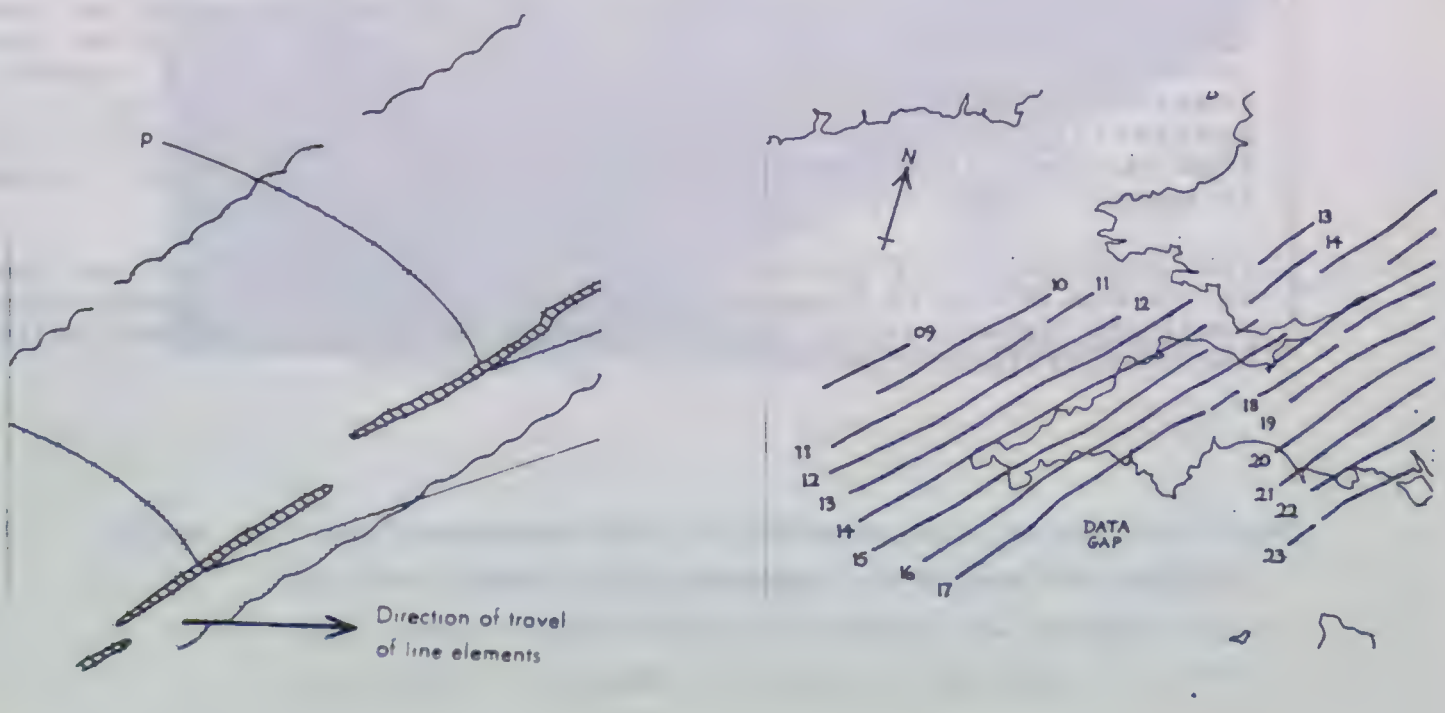

g. Post cold frontal rainbands, Type 5

These are typically 50 km wide, occur well behind the cirrus shield and are orientated parallel to the main cold front or occlusion. They are the only type of rainband easily recognised on satellite pictures; indeed this is often the best way to identify them. They consist of lines of loosely organised convective clouds and, on radar, the banded nature is often difficult to detect. An example of these bands is shown in Figure 30. Bennetts and Ryder 1983 suggest that these have a similar structure to Type 1 rainbnds in that a roll instability forms, but here, instead of having to overturn the atmosphere to produce convection, the air behind the front is already unstable. The roll therefore organises the convection into bands rather than permitting a more random release as is more usually seen in airmass convection. However it is important not to confuse these type of bands with secondary cold fronts.

It is instructive to return to table 1 and to notice the way in which the various bands have been grouped. Those classified as u-type tend to be associated with a roll type of circulation, with the heavier rain, which falls in a band, being generated by embedded convection. The D-type bands may also be of this form but sometimes the convection dominates and the bands become more severe and take the form of squall line. Finally the L-type bands are smaller bands. The narrow cold-frontal band is rather special in character and easily recognised and the other two types of rainband tend to appear as perturbations within u-type bands.

At present it is difficult to predict when and where the various types of bands will occur. For the smaller L-type bands and the convective dominated D-type bands, there is little chance of successful prediction from forecast models since the scale of the dominant mechanism is too small to be resolved. However for the dynamically dominated u-type, and the D-type in which the convection is weak, some progress can be made. Recent theoretical work suggests that the growth rate of the roll instability,which is the basis of these bands,may be predicted from the Met Office rectangle forecast model. An example of this is shown in Figure 31.

The prediction of growth rate is for the same time as the rainbands shown in Figure 26. It will be notice that the high predicted growth rates near the tip of Cornwall agree well with the observations of rainbands of Type 2 and 3b.

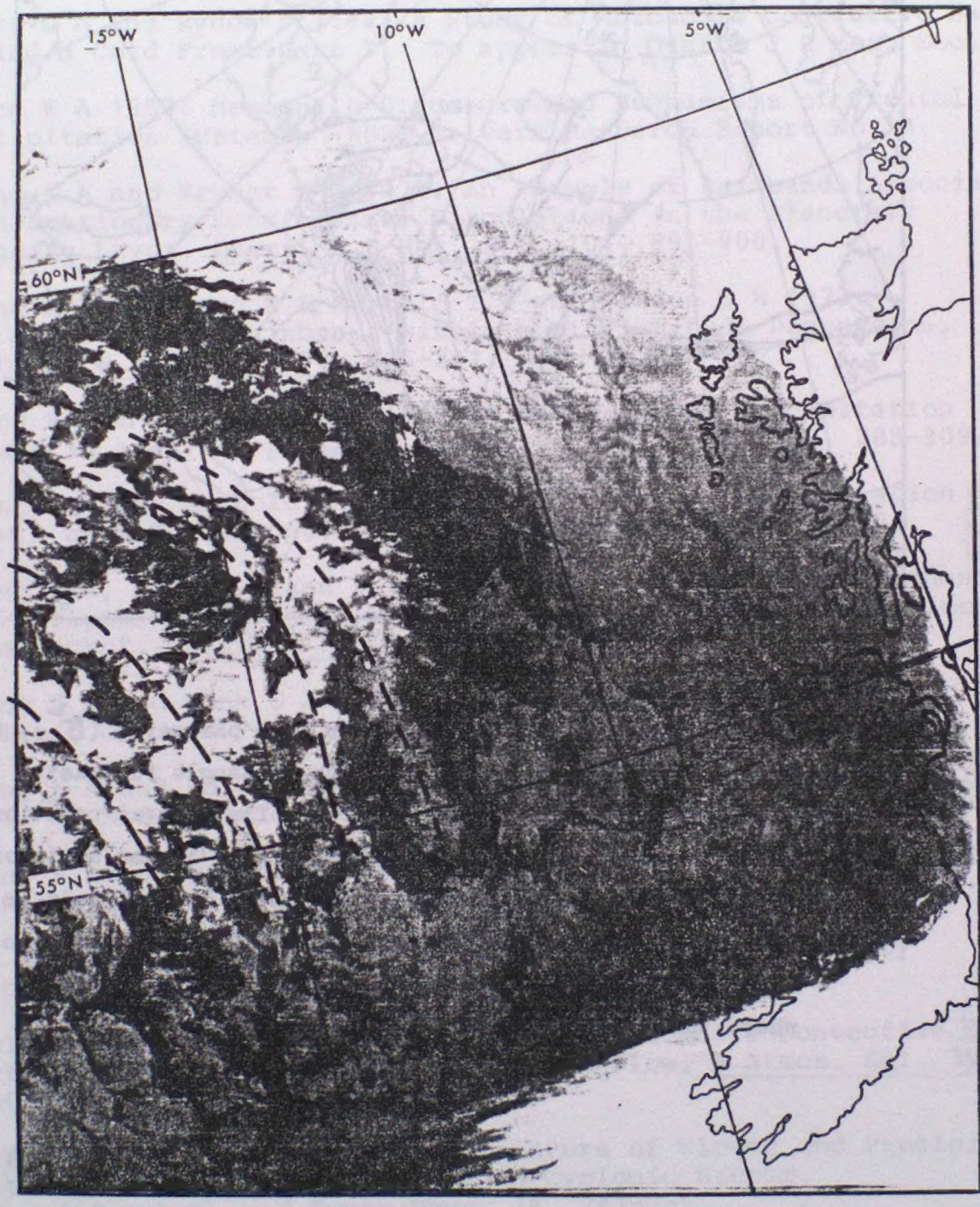

Figure 30. Type 5 rainbands behind an occluded front. On the North, East and South sides of the photograph can be seen the trailing edge of the occluded and cold fronts and the convective bands are visible in the cold air between 55 and 58 N, 12 to 18 W.

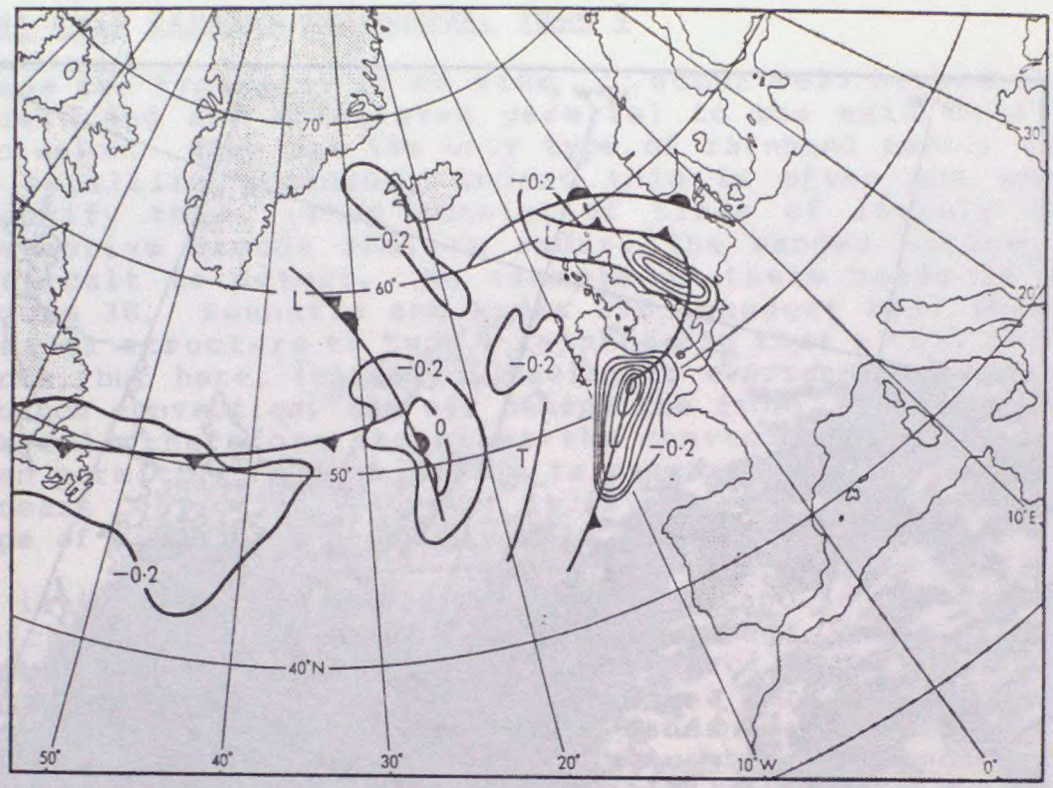

Figure 31. Spatial distribution of the growth rate parameter (σ^2), at 00 GMT 29/07/79, evaluated from the rectangle forecast model, 12 hours after initialization. The frontal positions were taken from the working charts of CFO. σ^2 has units of hours^{-2} ; if = 0.5, disturbances double in amplitude in ~ 1 hour. Radar pictures for the same time are shown in Figure 26 . Rainbands are evident near the Scilly Isles where the groth rate parameter is a maximum.

Bennetts D A and Hoskins B J 1979: Conditional Symmetric Instability - a possible explanation for frontal rainbands, Quart. J R Met. Soc. 105, 945-962.

Bennetts D A and Sharp J C 1982: The Relevance of Conditional Symmetric Instability to the Prediction of Mesoscale Frontal Rainbands, Quart. J R Met. Soc. 108, 595-602

Bennetts D A and Ryder P 1984: A Study of Mesoscale Convective Bands Behind a Cold Front Part I. To appear in Quart. J R Met. Soc.

Browning K A 1983: Mesoscale Structure and Mechanisms of Frontal Precipitation Systems. RSRE Malvern Research Report No 34.

Browning K A and Bryant G W 1975: An Example of Rainbands Associated with Stationary Longitudinal Circulations in the Planetary Boundary Layer, Quart. J R Met. Soc. 101, 893-900.

Browning K A, Hardman M E, Harrold T W and Pardoe C W 1973: The Structure of Rainbands within a Mid-latitude Depression, Quart. J R Met. Soc. 99, 215-231.

Browning K A and Harrold T W 1969: Air Motion and Precipitation Growth in a Wave Depression, Quart. J R Met. Soc. 95, 288-309/

Browning K A and Harrold T W 1970: Air Motion and Precipitation Growth at a Cold Front, Quart. J R Met. Soc. 96, 369-389.

Browning K A, Hill F F and Pardoe C W 1974: Structure and Mechanism of Precipitation and the Effect of Orography in a Winter-time Warm Sector, Quart. J R Met. Soc, 100, 309-330

Browning K A and Monk G A 1982: A Simple Model for the Synoptic Analysis of Cold Fronts, Quart. J R Met. Soc. 108, 435-452.

Browning K A and Pardoe C W 1973: Structure of Low-level Jet Streams ahead of Mid-latitude Cold Fronts. Quart J R Met. Soc. 99, 619-638.

Browning K A and Pardoe C W and Hill F F 1975: The Nature of Orographic Rain at Wintertime Cold Fronts, Quart. J R Met. Soc. 101, 333-352

Cullen M J P 1983: Solutions to a Model of a Front Forced by Deformation. Quart. J R Met. Soc. 109 565-573.

Emanuel K A 1981: Inertial Instability and Mesoscale Convective Systems. Part II: Symmetric CISK in a Baroclinic Flow, J Atmos. Sci. 39 1080-1097.

Hobbs P V 1978: Organisation and Structure of Clouds and Precipitation on the Mesoscale and Microscale in Cyclonic Storms. Rev. of Geophys. and Space Phys. 16, 741-755

Hobbs P V and Biswas K R 1979: The Cellular Structure of Narrow Cold-frontal Rainbands, Quart. J R Met. Soc. 105, 723-727

Hobbs P V, Locatlli, J D, Matejka T J and Houze R A Jr. 1978: Air Motions, Mesoscale Structure and Cloud Microphysics Associated with a Cold Front, Proc. Conf. on Cloud Phys. and Atmos. Elec. Issaquah, Washington, pp 277-283.Amer. Met. Soc. Boston, Mass.

Hoskins B J 1971: Atmospheric Frontogenesis Models: some solutions Quart. J R Met. Soc. 97, 139-153

Hoskins B J and Bretherton F P 1972: Atmospheric Frontogenesis Models: Mathematical Formulation and Solution J. Atmos. Sci, 29, 11-37

Houze R A Jr, Hobbs P V, Biswas K R and Davis W M 1976: Mesoscale Rainbands in Extratropical Cyclones, Mon. Wea. Rev. 104, 868-878

Matejka T J, Houze R A Jr and Hobbs P V 1980: Microphysics and Dynamics of Clouds Associated with Mesoscale Rainbands in Extratropical Cyclones. Quart. J R Met. Soc. 106, 29-56.

Roach W T and Hardman M E 1975: Mesoscale Air Motions Derived from Wind Finding Dropsonde Data: the warm front and rainbands of 18 January 1971. Quart. J R Met. Soc. 101, 437-462.

Roberts P H and Soward P M 1978: Rotating Fluids in Geophysics. Academic Press 171-203

Wallace J M and Hobbs P V 1977: Atmospheric Science, Academic Press pp 467.